

Article

# Construction of a Cutting-Tool Wear Prediction Model through Ensemble Learning

Shen-Yung Lin \* and Chia-Jen Hsieh

Department of Mechanical and Computer-Aided Engineering, National Formosa University,  
Yunlin 63201, Taiwan; 11020130@gm.nfu.edu.tw

\* Correspondence: sylin@nfu.edu.tw; Tel.: +886-919-051127

**Abstract:** This study begins by conducting side milling experiments on SKD11 using tungsten carbide TiAlN-coated end mills to compare the surface roughness performance between two combinations of milling process parameters (feed rate and radial depth of cut), along with three ultrasonic-assisted methods (rotary, dual-axis, and rotary combined with dual-axis). The results suggest that the rotary (z-axis oscillation) ultrasonic-assisted method may provide better performance. Subsequently, this superior ultrasonic-assisted method was applied both with and without laser locally preheating assistance, respectively. Using a Taguchi orthogonal array, milling process parameters (spindle speed, feed rate, and radial depth of cut) were planned for experiments with the same cutting tool and the workpiece just mentioned above. The surface roughness serves as the objective function while being constrained by cutting-tool life. The characteristics of the smaller-the-better in the Taguchi method were applied to determine the optimal combination of process parameters. Based on the optimal milling process parameters obtained and the superior hybrid-assisted method adopted, milling experiments were repeatedly performed to collect the data on cutting force and cutting-tool wear. Feature engineering was performed on the cutting force signals, and different domain characteristics from both the time and frequency domains were extracted. Hereafter, feature selection by random forest and data standardization were further applied to feature extractions, and the data processing was thus completed. For the processed data, a cutting-tool wear prediction model was constructed by ensemble learning. This method leverages various machine learning regression models, including decision tree, random forest, extremely randomized tree, light gradient boosting machine, extreme gradient boosting, AdaBoost, stochastic gradient descent, support vector regression, linear support vector regression, and multilayer perceptron. After hyper-parameter tuning, the ensemble voting regression prediction was performed based on these ten mentioned models. The experimental results demonstrate that the ensemble voting regression model surpasses the performance of each individual machine learning regression model. In addition, this regression model achieves a coefficient of determination ( $R^2$ ) of 0.94576, a root mean square error (RMSE) of 0.24348, a mean squared error (MSE) of 0.05928, and a mean absolute error (MAE) of 0.18182. Therefore, the ensemble learning approach has been proven to be a feasible and effective method for monitoring cutting-tool wear.



**Citation:** Lin, S.-Y.; Hsieh, C.-J.

Construction of a Cutting-Tool Wear Prediction Model through Ensemble Learning. *Appl. Sci.* **2024**, *14*, 3811. <https://doi.org/10.3390/app14093811>

Academic Editors: Xichun Luo and Abhilash Puthanveettill Madathil

Received: 15 April 2024

Revised: 28 April 2024

Accepted: 28 April 2024

Published: 29 April 2024

**Keywords:** SKD11; rotary ultrasonic; laser preheating; machine learning; ensemble learning



**Copyright:** © 2024 by the authors. Licensee MDPI, Basel, Switzerland. This article is an open access article distributed under the terms and conditions of the Creative Commons Attribution (CC BY) license (<https://creativecommons.org/licenses/by/4.0/>).

## 1. Introduction

When the demand for new products rapidly emerges, bringing with it new mold requirements, manufacturers must efficiently design and produce molds while maintaining precision. Among the various mold requirements, SKD11 alloy tool steel is a widely used material for mold manufacturing. SKD11 finds extensive applications in the automotive, household appliance, and electronics manufacturing industries. It is a high-carbon and high-chromium alloy steel that exhibits exceptionally high hardness and toughness. This steel also incorporates elements such as molybdenum (Mo) and vanadium (V), giving

it wear resistance, low deformation, high fatigue strength, and impact resistance characteristics. These qualities make it one of the preferred materials for various applications, including stamping dies and plastic molds. Heat-treated SKD11 alloy tool steel can achieve a hardness of HRC 58-62. However, these excellent properties of SKD11 make it a difficult-to-cut material. Difficult-to-cut materials have poor machinability, high-cutting-power requirements, and tend to generate a significant amount of cutting heat, resulting in elevated cutting temperatures, reduced tool life, and decreased production efficiency.

As cutting-tool wear increases, the magnitude and fluctuation pattern of cutting forces also undergo variations. Cutting-tool wear can lead to irregular fluctuations in cutting forces, causing vibrations during the cutting processes. By analyzing the characteristics of cutting force fluctuations, the degree of the cutting-tool wear can be inferred, allowing for the prediction of remaining cutting-tool life. Therefore, in the process of establishing a cutting-tool wear prediction model, precise monitoring and analysis of cutting force fluctuations contribute to achieving real-time awareness of the cutting-tool condition, enhancing the stability and efficiency of the manufacturing processes.

The necessity of establishing a cutting-tool wear prediction model lies in enhancing the efficiency, quality, and safety of the manufacturing processes. By predicting cutting-tool wear, the production line can promptly initiate cutting-tool replacement, thereby reducing downtime and production costs. Furthermore, the cutting-tool wear prediction model can be employed to optimize cutting parameters, improving machining efficiency. This helps prevent excessive wear or premature cutting-tool replacement, thus saving costs and extending cutting-tool life.

With the advancement of the times and the rapid development of technology, product iteration speeds have increased. At the same time, there is a need to deal with higher manufacturing complexity and shorter production cycles, which, undoubtedly, raise research and development costs, as well as production pressures in the industry. Finding more efficient and cost-effective ways to shorten production cycles is a challenge for the manufacturing sector [1,2].

The high strength, hardness, and toughness of SKD11 result in poor machinability. To meet the precision, stability, and shorter production cycles required for molds, there are numerous factors to consider during the machining process. These factors include, but are not limited to, machining parameters, machining assistance, and the impact of tool wear. Firstly, machining parameters such as cutting speed and feed rate play a crucial role. Cutting speed directly affects the machining time and tool wear rate, while the feed rate impacts material removal rates and surface roughness. Secondly, machining assistance significantly influence the machining process. Effective machining assistance can extend tool life and enhance product quality. Lastly, tool wear directly affects machining efficiency and workpiece quality. As tool wear increases, it results in reduced accuracy and increased surface roughness. Excessive tool wear can also lead to increased cutting forces, accelerating further tool wear and reducing production efficiency. Therefore, to improve the machinability of SKD11, enhance machining efficiency, and reduce production costs, it is essential to identify optimal process parameters and cutting assistance that can help minimize costs and improve machining efficiency [3].

A literature review on ultrasonic-assisted milling examines the influence of ultrasonic assistance on cutting performance. Kadhim Mejbil et al. [4] proposed axial ultrasonic vibration on the rotating mill to conduct experiments on hardened AISI H11 tool steel, using a carbide flat end mill. The experiments involved slot milling under wet cutting conditions with variations in cutting speed, feed rate, and milling depth in both conventional milling and ultrasonic vibration-assisted milling. The study aimed to investigate the effect of ultrasonic-assisted machining on surface roughness, surface topography, and subsurface microhardness. The results indicated that the surface produced by axial ultrasonic-assisted milling was uniform, and the peak-to-peak value remained consistent, thereby enhancing surface finish. Additionally, the study verified the importance of axial ultrasonic vibration on rotary tooling for improving machining surface quality, as this vibration imparts a

hammering action on the cutting-tool tip, making the cutting marks left by the teeth flat. Compared to conventional milling, ultrasonic-assisted milling resulted in a significant reduction of surface roughness,  $R_a$ , with up to 89.7% improvement. Tsai et al. [5] utilized cemented carbide flat end mills to conduct the ultrasonic-assisted end milling of AISI420 mold steel by varying the ultrasonic vibration frequencies and amplitudes, the rake angles and helix angles of the cutting-tool. The study aimed to improve machined surface roughness and cutting-tool wear via the assisted system. In addition, the effects of the input voltage, cutter stretch length, and holding force on the amplitude of the ultrasonic vibration system were also investigated. The results showed that the ultrasonic amplitude increased with increasing stretch length and input voltage. In addition, a proper holding force and an optimum amplitude, which are related to the best surface finish, were ascertained. The machined surfaces with ultrasonic-assisted milling exhibited better uniformity and smoothness as compared to those machined under the same conditions without assistance. In addition, the cutting-tool wear was slower during ultrasonic-assisted milling, which leads to an extension of tool life. Cutter geometry, such as positive rake angle with a larger helix angle of  $45^\circ$ , and vibration parameters, such as a frequency of 50 kHz and an amplitude of  $2.2 \mu\text{m}$ , provided better surface smoothness and smaller cutting-tool wear during ultrasonic-assisted milling. Ding et al. [6] investigated cutting machinability improvement in two-dimensional ultrasonic-assisted micro-end-milling on hardened tool steel. By varying the vibration parameters, such as amplitude and the frequency of ultrasonic assistance, experiments were conducted for both conventional and ultrasonic-assisted milling to examine their effects on surface roughness and cutting-tool wear under process parameter conditions. The results showed that cutting-tool wear in ultrasonic-assisted milling was reduced by approximately 5 to 20%. As the amplitude and frequency of the ultrasonic-assisted system increased, both cutting-tool wear and surface roughness decreased. Compared to conventional milling, this two-dimensional ultrasonic assistance effectively enhanced the overall machining performance. Gao et al. [7] performed the dry milling of Ti-6Al-4V with the assistance of longitudinal ultrasonic vibration to enhance machinability and surface quality. By varying the ultrasonic amplitude, an investigation was made with respect to cutting forces, cutting temperature, surface topography, and 3D surface roughness. The results showed that the average cutting forces along the feed and longitudinal direction, the maximum and average cutting temperature and the mean values of 3D surface roughness,  $S_a$  and  $S_q$ , all exhibited reductions from a specific percentage to a larger extent, respectively, as the ultrasonic amplitude increased from 0 to  $6 \mu\text{m}$ . These are attributed to the increased amplitude, which increased the separation distance between the cutting-tool and the workpiece, with friction constraint and contact time between them being thus reduced.

A literature review on laser-assisted milling examines the effect of thermal preheating on cutting performance. Kumar and Melkote [8] compared the advantages of laser-assisted micro milling on process responses, such as material removal rates, cutting-tool wear, cutting force, and surface finish. They utilized TiAlN-coated tungsten carbide end mills to perform micro slot milling experiments on A2 tool steel (62 HRC), with and without laser assistance, under a proper micro milling condition. The results showed an average reduction in cutting force of up to 69% with laser assistance. They also indicated that cutting-tool wear is significantly less with laser assistance, even when the material removal rates are increased by six times higher than the cutting conditions recommended by the tool manufacturer. Through the proper selection of cutting-tool diameter relative to laser spot size to handle the proper laser thermal preheating, better surface roughness and reduced cutting-tool wear can be obtained due to reduced burr height formation. Brecher et al. [9] studied the impact of laser-assisted milling on advanced materials' cutting forces and tool flank wear without cooling lubricants. They proposed an innovative laser-assisted equipment that guides the laser beam through an HSK tool interface, directing irradiation onto the cutting surface of the workpiece in the machining area. The milling experiments were conducted on Inconel 718, using cemented carbide end mills with TiAlN coatings on

a 5-axis machining center. The results showed that the cutting forces along  $F_x$ ,  $F_y$ , and  $F_z$  directions were reduced by 40%, 60%, and 60%, respectively, for the local plastification of workpiece material in laser assistance. Laser assistance may effectively reduce the cutting forces and flank wear with optimized laser parameters. Woo and Lee [10] studied the machining characteristics of laser-assisted milling on cylindrical shape workpieces, focusing on AISI 1045 and Inconel 718. They proposed a method for three-dimensional laser-assisted milling suitable for cylindrical workpieces and investigated its effects on surface roughness and cutting forces. Firstly, finite element analysis was conducted for both materials to determine the proper preheating temperature and effective cutting depth. Subsequently, milling experiments were performed, comparing them with conventional milling to observe variations in surface roughness and cutting forces. The results showed that finite element analysis for thermal analysis was effective in similar machining processes. Compared to conventional methods, laser-assisted milling significantly reduced cutting forces and surface roughness by some specific extent for AISI 1045 and Inconel 718. Additionally, as the milling position angle increased, both cutting forces and surface roughness increased. It was suggested to rotate the workpiece clockwise to decrease the angle or utilize tool edge machining to improve surface roughness and tool life. For AISI 1045, cutting forces decreased and surface roughness improved with three-dimensional laser assistance, while for Inconel 718, down milling demonstrated better results.

In their related literature review on high-speed milling, Wang et al. [11] utilized the split Hopkinson pressure bar technique to obtain stress-strain curves under high temperature and high strain-rate conditions. They also considered the negative strain rate and temperature effects of the material to modify the traditional empirical Johnson–Cook constitutive equation for SKD11 hardened steel. Based on the modified Johnson–Cook constitutive equation, they proposed a two-dimensional plane-strain finite-element model, coupled with thermal and mechanical loads for high-speed milling of SKD11. The FE model aims to simulate the geometric characteristics of chip formations during the high-speed milling processes and conduct the stress-and-strain quantitative analyses in the shear band. The cutting forces, cutting temperatures, and cutting performance of coated tools are also analyzed in the model. The results indicated that a critical value of cutting speed exists within a specific range. At this speed, stress and strain values increase, causing changes in stress and strain distributions in the shear band. This leads to the formation of a sawtooth chip. As the cutting speed continued to increase, the stress, strain, and temperature values in the shear band also increased, while the distribution in chip region remained unchanged, resulting in a more pronounced sawtooth chip pattern. The cutting forces decreased as the cutting speed increased, with temperature exerting a significant influence on cutting forces. The greater the temperature difference, the faster the decrease in cutting forces. Wang et al. [12] used TiAlN- and TiSiN-coated carbide tools for the high-speed milling of hardened steel to determine the wear and breakage mechanisms of the cutting-tool. The effects of the tool angle, diameter, extended length, cutting forces, and cutting-induced vibrations on tool conditions were also investigated. The results showed that the primary patterns of tool wear observed included flank wear, rake face wear, breakage, and micro-chipping. The breakage modes were coating peeling, chipping, and tip breakage. Increasing the tool extended length led to increased cutting forces and tool wear, thereby decreasing surface quality. The abnormal states that occurred after tool wear could be detected through the signals of cutting forces and cutting-induced vibrations. The TiSiN-coated tools had a significantly longer tool life compared to the TiAlN-coated tools. Furthermore, experiments revealed that using cutting tools with a smaller rake angle, a smaller right clearance angle, and a large helix angle effectively reduced cutting forces, extended tool life, and facilitated smoother cutting processes. Gong et al. [13] conducted milling experiments on H13 steel and SKD11 hardened steel by using coated carbide tools to investigate the tool wear and breakage mechanisms. The results indicated that the hardness of the workpiece had a dominant effect on tool failure patterns. In milling H13 steel, the tool failure pattern is flank wear, while in milling SKD11 hardened steel, tools were prone to breakage of the

rake face due to the initiation and propagation of cracks. Furthermore, the geometry model of tool wear and breakage was established to explore the variations in cutting-tool angles resulting from the tool's wear or breakage mechanisms. Flank wear in H13 reduced the working clearance angle, while the breakage of the rake face in SKD11 reduced the working rake angle. Additionally, the effects of tool wear and breakage on cutting forces and chip formation were analyzed. In milling H13 steel, flank wear increased the friction coefficient between the tool and the workpiece, leading to increased cutting forces and the formation of wave-shaped chips. In contrast, in milling SKD11 hardened steel, the breakage of the rake face increases chip deformation and reduces the sharpness of the cutting edge, resulting in the curling and separation of sawtooth chips. Pu and Singh [14] conducted high-speed ball nose end milling experiments on AISI A2 tool steel using PCBN and coated tungsten carbide tools on a 5-axis machining center, with variations in milling length and cutting speed to assess changes in the tool wear mechanism and surface roughness. The results revealed that coated carbide tools performed poorly within the high-speed machining range, while high-CBN-content PCBN tools are relatively suitable for this hardened steel. Under normal cutting speeds, the surface roughness of coated carbide tools was twice that of the PCBN tools. In addition, it led to work hardening on the workpiece, increased hardness, material drag, surface cracks, and microstructural changes. The failure mode of PCBN tools is flaking and edge chipping due to the fact that toughness is insufficient for application when the cutting edge is worn out. Moreover, low-CBN-content PCBN tools lack of the required toughness and abrasion resistance for the application. Gong et al. [15] conducted high-speed face milling of the hardened steel SKD11 to investigate the failure patterns and failure mechanism of a double-layer-coated cemented carbide tool. Additionally, the effects of cutting-tool damage on cutting forces, surface roughness, and tool failure surface morphology were also studied. The results showed that the dominating failure pattern of the coated tool in this study was fatigue fracture, accompanied by chipping. At low cutting speeds, many fatigue cracks were observed on the rake face, while fatigue striations and river patterns were observed at the fatigue crack propagation zone with the increase in cutting speed. In addition, fatigue steps and secondary cracks were found on the fatigue propagation area under higher cutting speeds. The main fracture modes were intergranular and transgranular fractures at lower and higher cutting speeds, respectively. The cutting force had a large influence on tool life in the initial tool wear stage. However, when the tool breakage and coating peeling occurred, the cutting temperature was the dominating factor for tool life. With increased flank wear and cutting forces, the values of machined surface roughness constantly increased.

With regard to the literature review on machine learning, Twardowski et al. [16] applied two different forms of machine learning classification trees to conduct a study, utilizing vibration acceleration measurements as the physical parameters, to predict the possibility of tool wear during the milling process of EN-GJL-250 cast iron. The experiments were carried out using a four-edge cemented-carbide end mill cutter, with vibration acceleration serving as the input data for the models to forecast tool wear. The study obtained the vibration acceleration results during the experiments and utilized machine learning techniques, particularly decision trees, to classify tool wear conditions. The experimental results showed that, compared to regression models, machine learning methods exhibited significantly smaller errors in predicting tool wear than those reached by the regression model. Niu et al. [17] used different machine tools conducting two milling-tool life tests to collect cutting performance data, such as cutting force, vibration, and cutting sound to construct a tool-wear monitoring model of titanium alloy milling. In the experiments, the above-mentioned raw signals were captured by multiple sensors and features were extracted on time, frequency, and time-frequency domains. Then, feature dimensionality reduction was achieved using an information measurement-based feature selection method, introducing symmetrical uncertainty to select relevant features. Finally, a multiclass support vector machine model was developed to identify the wear stages of the tool. The results demonstrated that the classifier using multiple sensors achieved an overall identification

accuracy of 96.7%, while the classifiers based on single-force sensors and vibration sensors exhibited performances of 96.7% and 92.5%, respectively. Mahmood et al. [18] conducted a study on the prediction of tool wear in various machining processes using machine learning. They performed different machining experiments such as milling, drilling, and turning for IN718 material, and each machining process employed six tools in different states of wear. Initially, experimental data on cutting force from three machining processes were utilized to extract 15 features. Subsequently, singular spectrum analysis and principal component analysis were employed for feature selection and dimensionality reduction, respectively. The severity of tool wear was categorized into five levels, and a prediction was performed using LightGBM and an ensemble model combining six algorithms: LR, RF, CART, NB, SVM, and KNN. The results demonstrated the outstanding performance of the LightGBM model in terms of speed and efficiency, effectively handling huge datasets. Additionally, the model overcame some of the deficiencies present in previous tool wear models, such as high dimensionality and overfitting. This improvement is attributed to the application of dropout and early stopping techniques. Zhou et al. [19] proposed a milling tool wear prediction method for multi-condition classification and rapid selection of prediction models based on linear discriminant analysis (LDA) and the ensemble method. First, the whole wear process of the cutting tool is divided into five stages. Next, the time domain, frequency domain, and wavelet packet of the raw data are extracted, and the RF and XGBoost algorithms are used for multi-algorithm feature screening. The LDA algorithm is used to fuse and downscale the screened features, which are then combined with the K-means clustering algorithm to group similar working conditions. The samples are expanded and balanced using the SMOTE algorithm. Then, separate regression and classification prediction models are created for each group of working conditions. These models are integrated with an algorithm to determine the optimal prediction model for each group of working conditions. Compared with the traditional transfer learning algorithms, the proposed method allows for the rapid selection of a prediction model, which is achieved by dividing new conditions into groups with reduced dimensionality. The test results demonstrate the method's effectiveness in addressing the challenges of selecting prediction models and reducing the number of model transfers. Kilundu et al. [20] explored the use of data mining techniques for monitoring the tool condition in metal cutting. The study focused on the analysis of vibration signals, particularly employing the pseudo-local singular spectrum analysis (SSA) method. The methodology includes the integration of SSA and band-pass filtering to process vibration signals, aiming to eliminate irrelevant noise components. A major advantage of this approach is its ability to extract relevant information from high-frequency vibration components. Additionally, the study explores the use of the SSA method to define features that are highly sensitive to tool wear, enabling the monitoring of tool condition. The results demonstrate that this method exhibits a high recognition rate in identifying tool wear conditions. However, its recognition rate is lower for dysfunctions in the cutting process, such as chip jamming and unproductive passes. This highlights the potential application of data mining techniques in tool condition monitoring. Huang et al. [21] proposed an indirect tool-wear measurement method based on multi-information fusion by hybrid machine-learning techniques, to increase the utilization efficiency of multi-sensor signals and improve the measurement accuracy of tool wear. Triaxial cutting forces and vibration signals are collected and then preprocessed by wavelet packet denoising. The time, frequency, and time-frequency domain features are extracted to reduce information redundancy, and the kernel principal component analysis is applied to fuse the most sensitive characteristics. A fusion model combining least squares support vector regression and particle swarm optimization algorithms is established to learn the dependency relationship between the fused features and tool flank wear. They conducted milling experiments under multiple working conditions to validate the effectiveness of the proposed method. The experimental results show that the overall performance of the proposed method is superior to that of other comparison methods.

Cutting forces play a crucial role in the machining process, providing vital information about the cutting tool's condition, being widely applied in various aspects of manufacturing. Firstly, by monitoring the changes in cutting force, effective cutting-tool wear monitoring can be achieved. As the cutting tool wears down, the magnitude and trends in the cutting force undergo fluctuations, and feature extraction of the cutting force can be used for analyzing the cutting tool's condition. Secondly, vibration analysis of cutting forces can be utilized to assess the stability of a machine tool, thereby detecting the presence of vibrations or resonances. Additionally, abnormal variations in cutting forces may indicate collisions between the tool and the workpiece or fixture, facilitating collision detection to ensure production stability and prevent damage. Cutting force data can also be employed for optimizing cutting parameters by establishing cutting force models to enhance processing efficiency and quality.

Machine learning and ensemble learning techniques have demonstrated excellent performance in constructing cutting-tool wear prediction models. Machine learning can automatically learn and extract complex features, enhancing the model's generalization capability. Ensemble learning, combining predictions from multiple models, effectively overcomes the limitations of individual models, thereby improving the overall predictive performance. Through these technologies, it can more accurately predict the trends in cutting-tool wear variations, achieving precise control over the cutting processes. Cutting force is a complex nonlinear function influenced by various factors, such as material properties, cutting-tool geometry, and cutting conditions. Utilizing cutting force as input parameters for prediction models comprehensively reflects the characteristics and variations of the cutting processes. By establishing cutting-tool wear models, the production line can promptly initiate cutting-tool replacement, thereby reducing downtime and production costs.

This study aims to identify the better assisted milling technology and optimal process parameter combinations for SKD11 hardened steel to enhance cutting performance and machining quality. Based on these foundations, a cutting-tool wear prediction model through machine learning is further developed to improve the production efficiency and cost reductions. The model can predict cutting-tool wear in real-time, reducing the replacement times of premature tool disposal, enhancing the rate of high-quality products, minimizing the degradation of cutting quality due to excessive tool wear, and further enabling intelligent automatic cutting-tool changing. The goal is to achieve automated and intelligent manufacturing that maintains both product quality and high efficiency in the production of hardened steels.

## 2. Theoretical Foundation

### 2.1. Cutting-Tool Wear

The cutting-tool wear processes may be divided into three stages: (1) initial wear; the cutting edge is relatively rough in this stage, and the contact area among the cutting tool, workpiece, and chips is small. The cutting forces are concentrated at the cutting edge, leading to a relatively rapid cutting-tool wear in this stage. (2) Normal wear; after the initial wear occurred in the first stage, the cutting edge gradually becomes smoother, and the contact area among the cutting tool, workpiece, and chips increases. As a result, cutting forces are not concentrated at the cutting edge, leading to a slower wear rate. The cutting tool enters a phase of normal wear during this stage. (3) Severe wear; when wear progresses to a certain extent, the machined surface becomes rough, and the friction between the cutting edge and the workpiece increases. The rise in cutting forces and temperatures leads to an accelerated wear rate. At this point, the cutting edge loses its ability to remove the workpiece material effectively. The relationship between cutting-tool wear and machining time for these three stages is depicted in Figure 1.

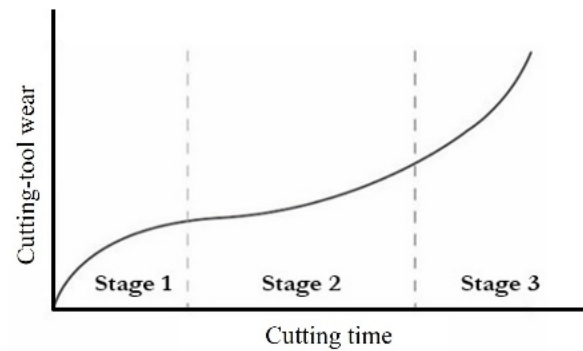


**Figure 1.** Cutting-tool wear processes.

## 2.2. Machine Learning

Machine learning is a critical branch of artificial intelligence that has seen extensive application in recent years, including our daily lives. In recent times, machine learning has also gained considerable attention and application in the industrial sector. According to retrospective studies [22], it can be used for equipment anomaly detection, equipment monitoring, early prevention of equipment failures, reducing downtime, lowering maintenance costs, and improving production efficiency, all of which hold significant importance. The core objective of machine learning is to address complex problems, build models capable of learning from large volumes of data, and discover patterns within the data. It can be broadly categorized into four main types: (1) supervised learning; supervised learning primarily involves training models using labeled training data. The model learns the underlying relationship between inputs and outputs, enabling it to predict the desired output from input data. (2) Unsupervised learning; in contrast to supervised learning, unsupervised learning does not require labeled training data. It classifies and clusters data based on relationships or similarities among data points. (3) Reinforcement learning; reinforcement learning allows models to learn through interaction with their environment. Models adjust their behavior based on rewards or penalties received for their actions. This type of learning is suitable for scenarios where models need to learn through trial and error, closely resembling human learning. (4) Semi-supervised learning; semi-supervised learning is a combination of supervised and unsupervised learning. It involves training on both labeled and unlabeled data to improve prediction accuracy.

Different machine learning methods have their strengths, weaknesses, and suitable application scenarios. The choice of which method to use should be based on the task objectives and context assessment.

## 2.3. Ensemble Learning

In the application of machine learning, the ideal scenario involves training a single model that learns the patterns or underlying rules within the provided data and makes accurate predictions for the task at hand. However, in reality, this is often not the case. The complexity of data, imbalanced data distributions, and the presence of significant noise, among other factors, make it challenging for a single model to achieve ideal predictive outcomes. As per the research presented by Sarker [23], these challenges can limit the performance of a single model.

Ensemble learning is a machine learning strategy that combines predictions from multiple machine learning models to improve overall predictive accuracy. According to a review study [24], ensemble learning can enhance generalization capability by training multiple models and combining their predictions. It has found wide application across various domains. The following are some common ensemble methods, including bagging, boosting, stacking, and voting. (1) Bagging is based on random sampling from the raw data to create multiple different training datasets. Several models are then trained on these datasets, and the predictions from each model are averaged or voted on to enhance model performance. Random sampling is achieved through the bootstrap method, where

subsets are randomly selected, with replacement, from the raw data. For classification problems, the final output is determined by voting according to the predictions of each model. For regression tasks, the final output is the average of the predictions from the models. (2) Boosting is an iterative ensemble learning method. It relies on adjusting sample weights and iteratively optimizing the model. Each round of learning depends on the previous round's results. Errors in predictions are given higher weights to improve performance in the subsequent round. Each model learns from and corrects errors in the previous model, resulting in improved predictive accuracy. (3) Stacking aims to combine the strengths of multiple base models. This approach first trains multiple different base models, and the final output is derived from a meta-learner that is trained on the predictions of the base models and their correspondence with the true values. This method leverages the power of multiple models to enhance overall predictive accuracy. (4) Voting combines predictions from multiple models. For classification tasks, each model makes predictions, and the final output is determined by majority voting. In regression problems, the final prediction is the average of the base models' predictions. Voting can be effective when the base models have different strengths and weaknesses, allowing them to complement each other.

Ensemble learning is widely applied and studied in the field of machine learning. It leverages the combination of different machine learning models to enhance predictive capabilities and achieve more accurate results.

### 3. Approach Methods and Procedures

The side milling experiments of SKD11 alloy tool steel conducted in this study may be divided into two phases. The 1st phase tries to explore a better ultrasonic-assisted method for further application in the 2nd phase. Locally, laser preheating assistance is additionally incorporated with better ultrasonic-assistance to constitute hybrid-assisted milling, in which process parameter combinations are planned based on Taguchi orthogonal arrays. In addition, the optimal process parameter can be determined by the Taguchi method. This study aims to investigate and analyze the influence of milling process parameters and different assisted machining methods on surface roughness, surface morphology, and cutting tool wear. Finally, experiments were repeatedly conducted by using the optimal cutting parameter combination and a hybrid-assisted system to collect the data of cutting force and cutting-tool wear. Based on these data, a cutting-tool wear prediction model is constructed through the ensemble learning method. The entire procedure executed in this study is illustrated in Figure 2.

#### 3.1. Milling Experimental Setup

This study aims to explore various assistance methods and process parameters for SKD11 milling. The investigation is divided into two phases. In the first phase of the milling experiment, the focus is on the analysis of cutting performance with no assistance, rotary ultrasonic assistance, dual-axis ultrasonic assistance, and a combination of rotary and dual-axis ultrasonic assistance (triple-axis ultrasonic). In the second phase, based on the results of the first phase analysis, a better assistance method is selected for the second phase of the milling experiment. The milling parameters are planned by using an L9 orthogonal array. During the experiment processes, observations and measurements are made for surface roughness, cutting forces, surface morphology, and cutting-tool wear. A series of result analyses and discussions are conducted.

The first phase of the experiment aims to explore the effects of different ultrasonic-assisted methods, namely rotary, dual-axis, and triple-axis, on milling performance. In this phase, two sets of process parameters are planned, as shown in Table 1. These two sets of process parameters, with or without assisted methods, respectively, are all conducted in the experiment, and a total of 8 experiments are executed in this phase. Two factors with individually extreme levels were designated in this phase.

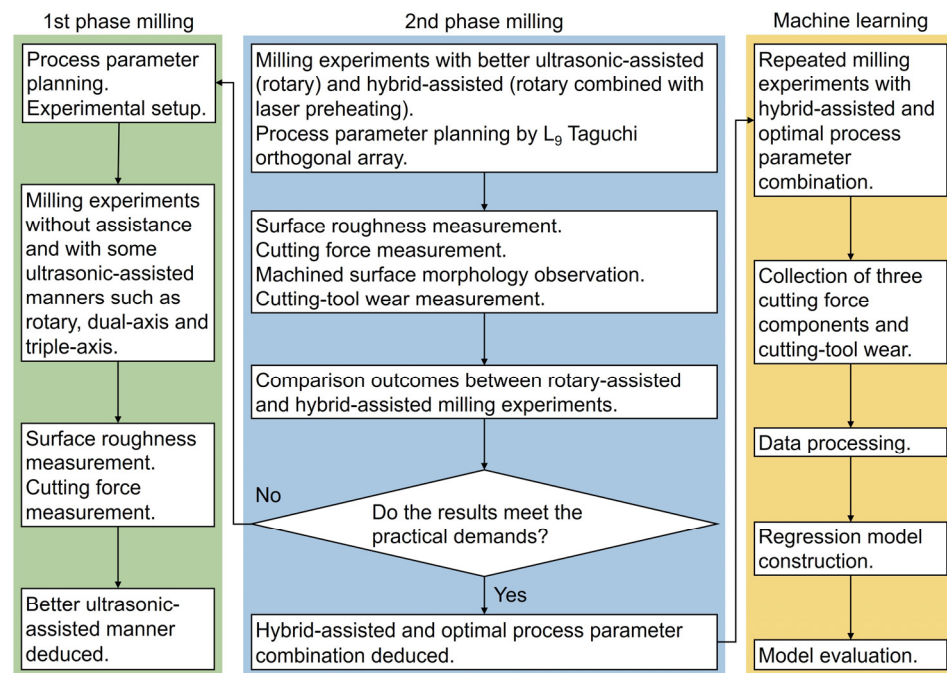


Figure 2. Entire list of procedures executed in this study.

Table 1. Process parameter planning for milling experiment of SKD11 in 1st phase.

Set	Spindle Speed, n (rpm)	Radial Depth of Cut, a <sub>e</sub> (mm)	Feed Rate, F (mm/min)	Axial Depth of Cut, a <sub>p</sub> (mm)
1	8000	0.1	1000	10
2	8000	0.3	1500	10

The superior ultrasonic-assisted method obtained from the first phase is adopted in the second phase both in conjunction with and without locally laser preheating assistance, respectively. The process parameter planning for the milling experiment of SKD11 is shown in Table 2. Three factors were considered, and each factor had three levels in the 2nd phase. The Taguchi orthogonal array was applied to design milling process parameter combinations, resulting in a total of 18 experiments, as shown in Table 3. Surface roughness and cutting-tool life serve as the objective function and constraint, respectively, and the optimal combination of process parameters was thus determined by the characteristics of smaller-the-better in the Taguchi method. Based on the optimal milling process parameters obtained and the superior hybrid-assisted method adopted, milling experiments were repeatedly performed to collect the data on cutting force and cutting-tool wear.

Table 2. Process parameter planning for milling experiment of SKD11 in the 2nd phase.

Milling Cutter Diameter, d (mm)	Φ6
Axial depth of cut, a <sub>p</sub> (mm)	10
Spindle speed, n (rpm)	8000, 9000, 10,000
Radial depth of cut, a <sub>e</sub> (mm)	0.1, 0.3, 0.5
Feed rate F, (mm/min)	1000, 1500, 2000

Based on the results from the second phase of the milling experiments, the optimal process parameters were determined to be a spindle speed of 10,000 rpm, a feed rate of 1000 mm/min, and a radial depth-of-cut of 0.1 mm, along with a hybrid-assisted method of rotary ultrasonic combined with local laser preheating. The experiments for data collection were conducted with these process parameters and assisted configurations.

Figures 3 and 4 show the milling experimental setup and a photo depicting equipment configurations. In this setup, rotary ultrasonic-assisted milling is controlled by adjusting the voltage levels through an ultrasonic driver, and the ultrasonic cutting-tool holder is driven by a non-contact power transmitter. The resonant effect was used to achieve the z-axis reciprocal oscillations at a high-frequency of 20 to 40 kHz. Laser assistance involves localized preheating of the workpiece surface by a laser spot through a laser tube. Data collection was performed using a dynamometer to capture cutting force signals along the x, y, and z directions. Through a charge amplifier, the cutting force signals were amplified and converted into voltage signals. Signal acquisition cards were used to capture the three cutting force components during machining processes at a sampling rate of 50 kHz, as shown in Figure 5a. Each data set of the cutting force signal consists of three portions for each force component during milling processes, i.e., before engagement, engagement, and after engagement. After each machining operation was completed, the cutting tool was photographed using a tool microscope, and its flank wear was observed and measured, as shown in Figure 5b. A total of 90 sets of cutting force signals and cutting-tool wear were collected for use in building subsequent regression models.

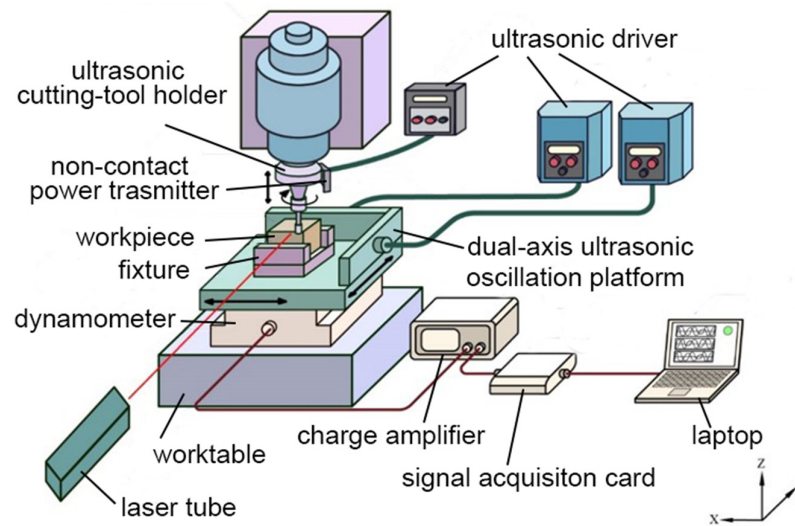


Figure 3. Milling experimental setup.

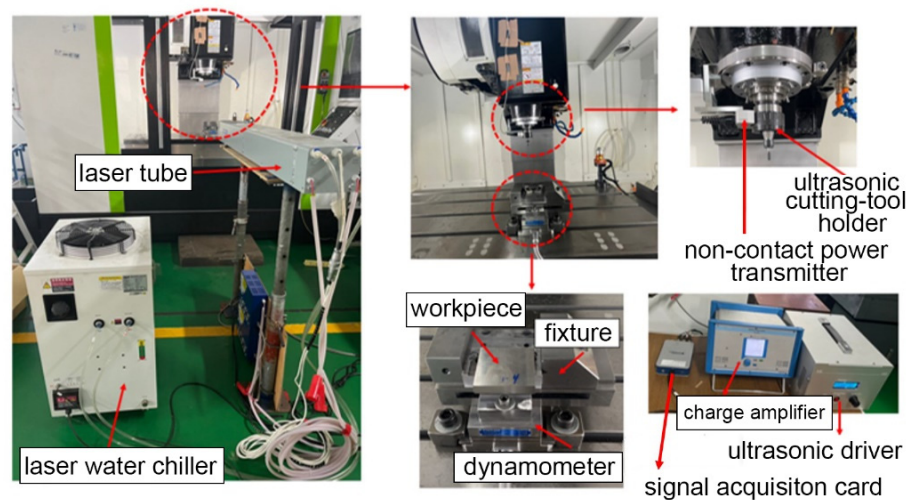
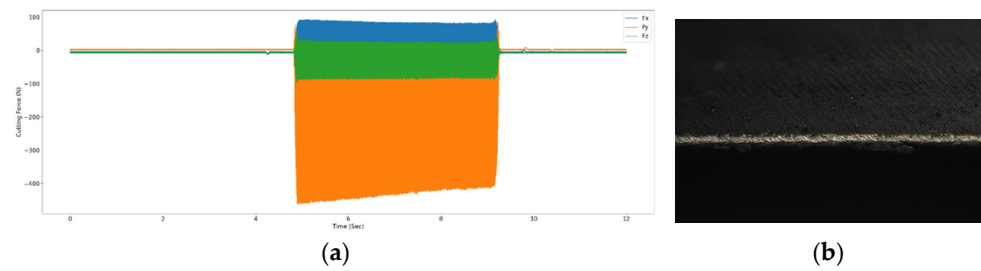


Figure 4. Photograph for experimental equipment configurations.



**Figure 5.** Three cutting force components and cutting-tool wear. (a) Three cutting force component signals. (b) Cutting-tool wear.

**Table 3.** Process parameter combinations by L9 orthogonal array in the 2nd phase.

Sets	Process Parameter	Spindle Speed Level	Radial Depth of Cut Level	Feed Rate Level
1	1	1	1	1
2	2	1	2	2
3	3	1	3	3
4	4	2	1	2
5	5	2	2	3
6	6	2	3	1
7	7	3	1	3
8	8	3	2	1
9	9	3	3	2

### 3.2. Machine Learning Architecture

This study, based on predicting cutting-tool wear using a better assisted milling method and milling process parameter combinations, consists of the following processes. First, the data collected in the milling experiments in Section 3.1 undergo data processing, including data cleaning, feature extraction, data splitting, data standardization, and feature selection. The purpose of these procedures is to prepare the proper data for constructing a variety of machine learning models. Second, the dataset is randomly split into an 80% training set and a 20% test set. Various machine learning models are constructed using the training set, with hyperparameter optimization and model evaluation conducted through grid search and cross-validation to optimize the basic models. Finally, an ensemble regression model is constructed, and it is evaluated using the test set data. The framework is illustrated in Figure 6.

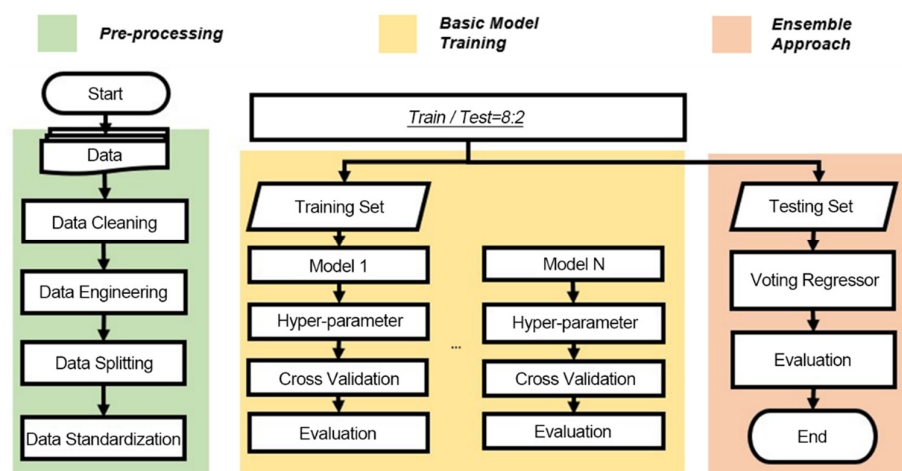


**Figure 6.** An architecture for machine learning processes.

### 3.3. Data Processing

In the experiments,  $x$ ,  $y$ , and  $z$ -axis cutting force signals were sampled, as shown in Figure 7. The raw cutting force signals include three portions, i.e., before cutting-tool engagement, the milling process, and after cutting-tool engagement. The signals before and after the cutting-tool engagement portions, highlighted by the red dashed boxes, are removed, while only the stable cutting force signals during the milling process, as indicated by the green dashed box, are reserved for use.

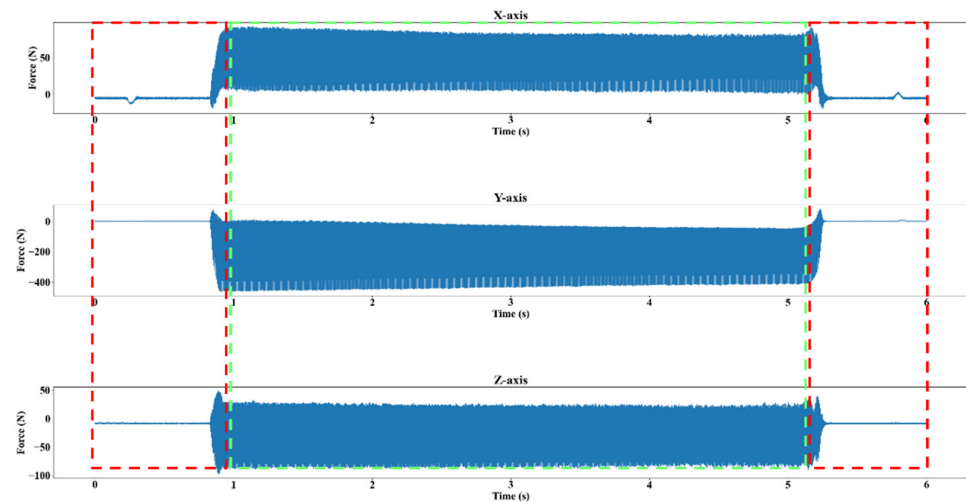


**Figure 7.** Three cutting force component signals sampled from experiments.

In a study investigating the relationship between cutting forces and cutting-tool wear [25], it was found that by performing a Fourier transform on the cutting force signals, changes in the amplitudes of rotational speed frequency, tooth passing frequency, and their harmonics were observed due to cutting-tool wear. Following this research, this study applied a Fourier transform to the cleaned cutting force signals to analyze them in the frequency domain, as shown in Figure 8. From the graph, it can be observed that the dominant frequencies are low-frequency signals, with a frequency of 166 Hz, associated with a spindle speed of 10,000 rpm and a frequency of 664 Hz, associated with the 4-flute end mill. The other frequencies are harmonics of spindle speed or tooth passing frequencies. Since the cutting force signals are predominantly low-frequency signals, a low-pass filter was applied to complete the data cleaning process.

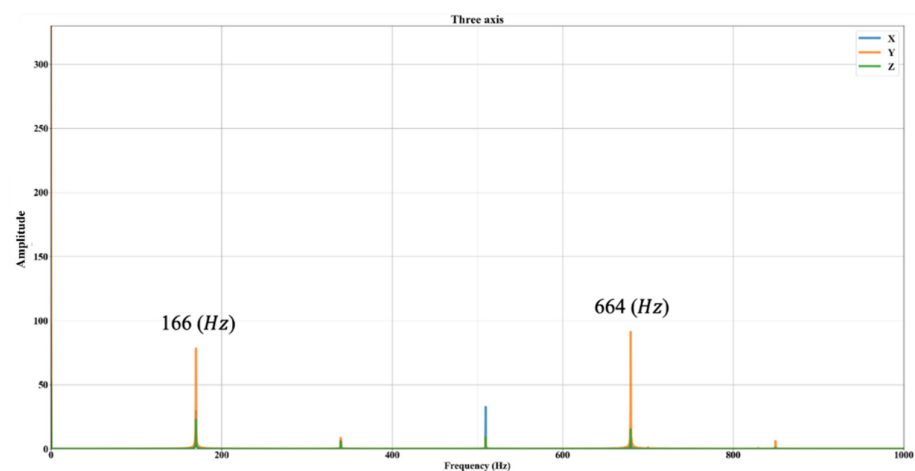


**Figure 8.** Three cutting force components exhibited in frequency domain.

The cutting force signals contain various environmental noises and, therefore, it is essential to extract significant features that reflect cutting-tool wear during the cutting

processes. As cutting-tool wear progresses, it affects the geometrical shape of the cutting edges of the end mill, which, in turn, impacts the contact area between the cutting-tool and the workpiece, resulting in increased cutting forces. Therefore, analyzing variations in cutting forces in the time domain can provide valuable insights into cutting-tool wear [26]. Moreover, variations in cutting forces also lead to variations in the frequency domain. Extracting features on frequency domain can also be used to assess the cutting-tool wear conditions [27]. Therefore, extracting features from different domains in the raw signals can effectively increase the relevance to cutting-tool wear [28,29]. In this study, feature extraction was performed on the cleaned cutting force signals, with their expressions, as indicated in Table 4. The sampling frequency for the cutting forces in this study was set at 50 kHz. Thus, each cleaned cutting force signal for one component contains approximately 200,000 data points. The relevant details are stated as follows:

1. For the  $x$ ,  $y$ , and  $z$  axes, 9 features in the time domain and 4 features in the frequency domain were extracted from the cutting force signals.
2. For the  $x$ ,  $y$ , and  $z$  axes, the cutting force signals were divided into 10 windows, with each window containing around 20,000 data points, as shown in Figure 9. Nine features in the time domain were then extracted for each window.
3. For the  $x$ ,  $y$ , and  $z$  axes, the cutting force signals were transformed into the frequency domain using a Fourier transform. The frequencies of spindle speed at 10,000 rpm and 4-flute tooth passing in the experiments were approximately 166 Hz and 644 Hz, respectively. Therefore, these frequencies within  $\pm 5$  Hz were extracted, and their amplitudes were used as features.

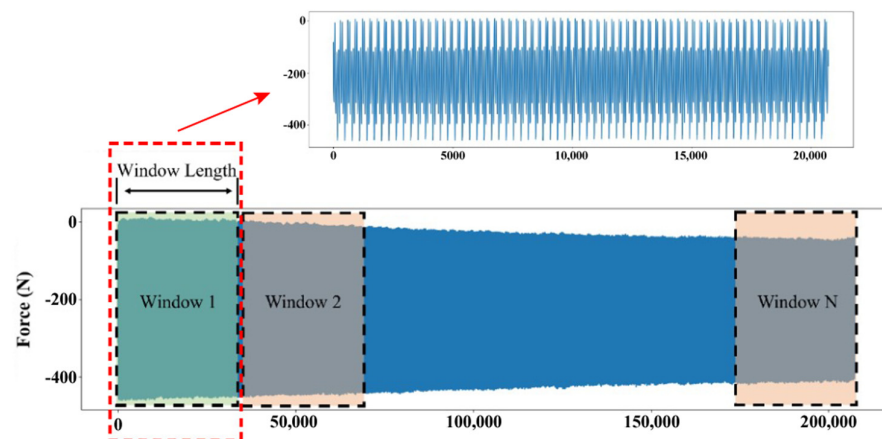


**Figure 9.** Segmentation on  $y$ -component cutting force signal.

After completing the data feature extraction, the dataset is randomly split into a training set and a test set, with an 80% and 20% ratio, respectively. Subsequently, data standardization is performed. Features from different domains may have varying scales or range differences. Standardizing the data ensures that all feature magnitudes are within the same range, facilitating better model training and evaluation. This reduces biases and errors introduced by differences in feature magnitudes, allowing the model to learn more about trends between numerical values.

In this study, Z-score normalization is utilized for data standardization. The Z-score is calculated using the formula shown in Equation (1), where the variables are defined as follows:  $z$  represents the standardized value,  $x$  denotes the raw data points after feature extractions,  $\mu$  corresponds to the mean of the dataset, and  $\sigma$  is the standard deviation of the dataset. After this processing, the mean of the standardized dataset is 0, and the standard deviation is 1.

$$z = \frac{x - \mu}{\sigma} \quad (1)$$

After standardizing the training and test data, feature selection is subsequently performed. Feature extraction is based on the three cutting force component signals after data cleaning, and it involves three main aspects:

1. For the cleaned cutting force signals, 9 time-domain features and 4 frequency-domain features were extracted.
2. Each cutting force component signal is segmented into 10 windows, and 9 time-domain features are extracted in each window.
3. The cleaned cutting force signals are transformed into frequency-domain, and the amplitudes correspond to spindle speed and tooth passing frequencies, and their harmonics are extracted.

After feature engineering, the extraction of features related to cutting-tool wear results in a relatively large number of features. Therefore, feature selection is conducted in order to find an optimal subset of features. Feature selection is a crucial step in machine learning, as an excessive number of features can lead to overfitting, causing a decline in prediction model performance. Through feature selection, irrelevant or redundant features can be eliminated, and those that contribute to predicting the target variable are retained. Reducing the number of features can also lower the computational cost of model training and prediction. In this study, the method employed for feature selection is based on the feature importance in random forests.

**Table 4.** Expressions for extracted features.

Domain	Feature	Expression
Time domain	Absolute maximum value	$x_{max} = MAX x_i $
	Mean	$\bar{x} = \frac{1}{N} \sum_{i=1}^N x_i$
	Variance	$x_{var} = \frac{1}{N} \sum_{i=1}^N (x_i - \bar{x})^2$
	Skewness	$x_{skew} = \frac{1}{N-1} \frac{\sum_{i=1}^N (x_i - \bar{x})^3}{x_{std}^3}$
	Kurtosis	$x_{kurt} = \frac{1}{N-1} \frac{\sum_{i=1}^N (x_i - \bar{x})^4}{x_{std}^4}$
	Peak-to-peak	$x_{p-p1} = x_{max} - x_{min}$
	Peak factor	$C = \frac{x_{p-p1}}{x_{rms}}$
	Pulse factor	$S_m = \frac{x_{p-p1}}{\frac{1}{N} \sum_{i=1}^N  x_i }$
	Waveform factor	$S_b = \frac{x_{rms}}{\frac{1}{N} \sum_{i=1}^N  x_i }$
Frequency domain	Average amplitude value	$S_1 = \frac{1}{N} \sum_{i=1}^N p_i$
	Center of gravity frequency	$f_c = \frac{\sum_{i=1}^N f_i p_i}{\sum_{i=1}^N p_i}$
	Mean square frequency	$ms_f = \frac{\sum_{i=1}^N f_i^2 p_i}{\sum_{i=1}^N p_i}$
	Frequency variance	$v_f = \frac{\sum_{i=1}^N (f_i - f_c)^2 p_i}{\sum_{i=1}^N p_i}$

#### 4. Results and Discussion

The side milling experiments on SKD11 were conducted in two phases to determine a better assisted method and optimal process parameters. In the first phase, eight experiments were carried out under two sets of process parameters both without assistance and with several ultrasonic-assisted methods, such as rotary, dual-axis, and triple-axis. This was undertaken to explore and identify the most effective assisted system. In the second phase, a superior ultrasonic-assisted method was further combined with or without assistance from local laser preheating to conduct L9 orthogonal array milling experiments, totaling

18 experiments. Thus, the effects of spindle speed, feed rate, and radial depth of cut, along with hybrid-assisted and rotary-assisted methods on surface roughness, cutting force, and machined surface morphology of SKD11 were investigated.

#### 4.1. Surface Roughness

Due to the high hardness and toughness of the SKD11 tool steel, various issues may arise during the machining process. Different assisted methods and machining parameters are crucial factors affecting machining performance. Table 1 shows the planning of process parameters in the first phase of the experiment, while Figure 10 shows the relationship between surface roughness and process parameter combination in this phase without assistance and with different ultrasonic-assisted methods. Here, the surface roughness parameter measured is Ra, and its measurement device is a contact-type surface roughness-measuring instrument (Mitutoyo SJ-410). The experimental results indicate that a small depth of cut and a slow feed rate result in better surface roughness than a large depth of cut and a fast feed rate, both without assistance and with different ultrasonic-assisted methods. Among them, the rotary ultrasonic-assisted method proves superior to both the absence of assistance and the other ultrasonic-assisted methods. However, the absence of assistance yields better performance than both dual-axis and triple-axis ultrasonic assistance. It is speculated that dual-axis and triple-axis ultrasonic assistance, which involve radial vibration, are less effective in removing material due to the high toughness property of the workpiece material. This deduction suggests poorer performance. Compared to no assistance, rotary ultrasonic assistance can reduce surface roughness by approximately 5%. Therefore, the effects of both no assistance and different ultrasonic-assisted methods on the surface roughness of SKD11 milling are investigated, and the best assisted method is ascertained. This superior ultrasonic-assisted method, rotary, will be applied in the second phase milling experiments.

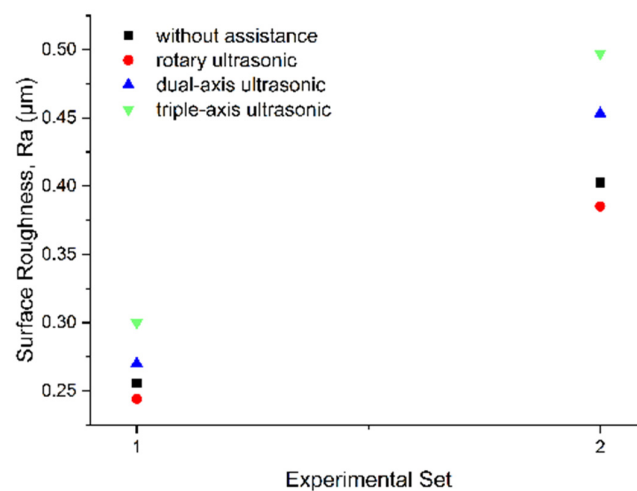


**Figure 10.** The relationship between surface roughness and process parameter combinations in the 1st phase experiment without assistance and with different ultrasonic-assisted methods.

The superior ultrasonic-assisted method obtained from the first phase is adopted in the second phase in conjunction with and without laser locally preheating assistance, hybrid-assisted, and rotary ultrasonic-assisted, respectively, in which the process parameter planning for the milling experiment on SKD11 is shown in Table 2. An ANOVA (analysis of variance) is performed on the sampling data to examine the influence and contribution of various factors to surface roughness. The contribution rates are shown in Tables 5 and 6, and the corresponding factor responses are illustrated in Figure 11a,b, respectively. It can be observed that under both of these assisted methods, the most significant factor affecting the surface roughness of SKD11 milling is the feed rate, followed by radial depth of cut, and lastly spindle speed. The experimental process parameter design for milling experiments

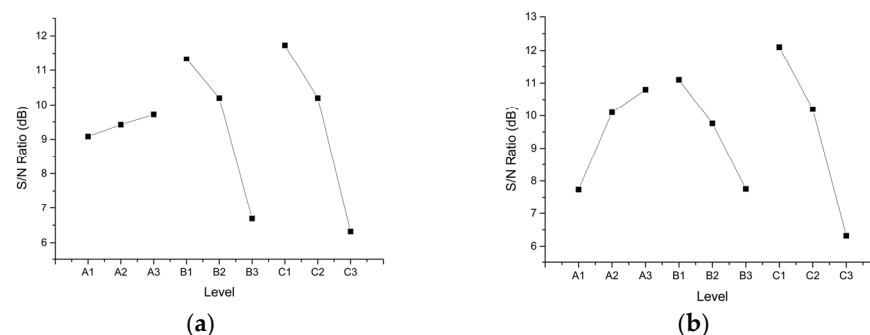
through L9 orthogonal arrays is presented in Table 2, and the corresponding experimental sets are shown in Table 3. Comparing surface roughness between hybrid-assisted and rotary ultrasonic-assisted methods for process parameter combinations in the L9 orthogonal array, as shown in Figure 12, it is evident that the hybrid-assisted method can reduce surface roughness by up to 30%, compared to rotary ultrasonic-assisted alone. Among them, lower feed rates result in better surface roughness. Higher feed rates may accelerate the cutting progression but may cause vibrations between the cutting edge and the workpiece surface, leading to deteriorated surface roughness. Meanwhile, a slower feed rate allows for an increase in laser preheating time during the cutting processes, effectively achieving a sufficient preheating phenomenon, and thereby enhancing the surface roughness of the machined surface.

**Table 5.** Variance analysis of surface roughness for rotary ultrasonic-assisted milling.

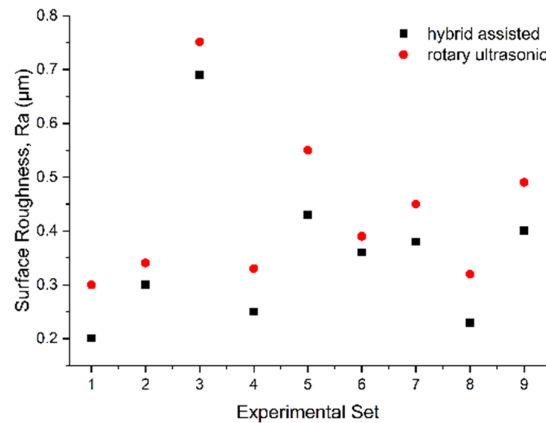
Factor	Factor Level (S/N)			Sum of Squares (SS)	Contribution Rate ( $\rho\%$ )
	1	2	3		
n (A)	9.08	9.42	9.71	0.6	0.72
$a_e$ (B)	11.33	10.2	6.69	35.2	42.65
F (C)	11.73	10.2	6.32	46.5	56.36
Error				0.22	0.27
Total				82.47	100.00

**Table 6.** Variance analysis of surface roughness for hybrid-assisted milling.

Factor	Factor Level (S/N)			Sum of Squares (SS)	Contribution Rate ( $\rho\%$ )
	1	2	3		
n (A)	7.74	10.1	10.8	15.1	17.65
$a_e$ (B)	11.1	9.76	7.76	16.6	19.45
F (C)	12.1	10.2	6.32	51.6	60.34
Error				2.19	2.56
Total				82.49	100.00



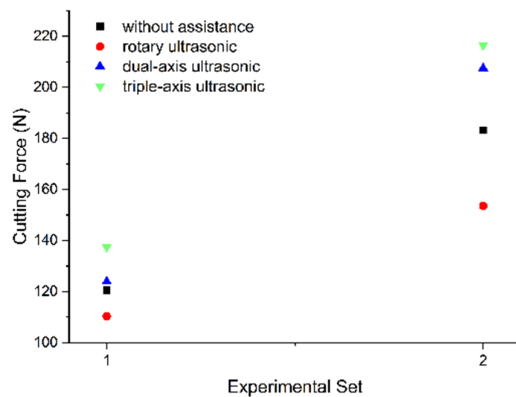
**Figure 11.** Factor response plot of surface roughness for rotary ultrasonic-assisted and hybrid-assisted milling. (a) Rotary ultrasonic-assisted. (b) Hybrid-assisted.



**Figure 12.** Surface roughness comparison between hybrid-assisted and rotary-assisted methods for process parameter combinations in L9 orthogonal array.

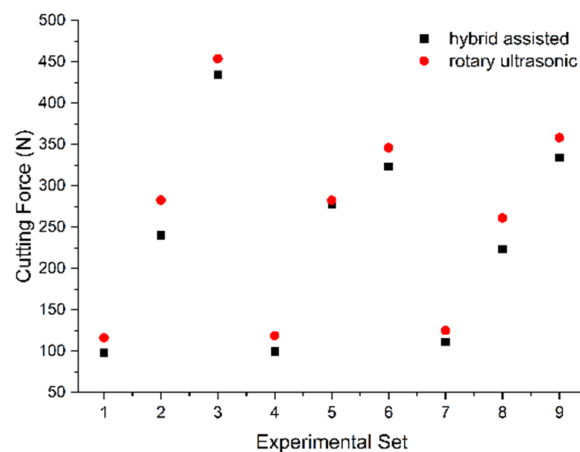
#### 4.2. Cutting Force

Figure 13 shows the cutting force comparison both among different ultrasonic-assisted methods and without assistance for two sets of process parameters planned for the first phase of the experiment. It can be observed that in the first phase of the milling experiment, the cutting force with triple-axis ultrasonic assistance is the highest, while the cutting force with rotary ultrasonic assistance is significantly lower than with the other assistances. The cutting force without assistance is lower than that with dual-axis and triple-axis ultrasonic assistances. Therefore, in this phase, it is evident that rotary ultrasonic assistance can effectively reduce cutting forces. It is speculated that since dual-axis and triple-axis ultrasonic assistance methods include radial vibration, the material’s high hardness and toughness prevent effective disruption of the material structure, leading to less effective material removal. Additionally, it increases the contact area and cutting load. In the case of triple-axis ultrasonic assistance, the radial vibration, unable to disrupt the workpiece material structure effectively, is combined with z-axis oscillation, increasing the contact area and cutting load compared to dual-axis ultrasonic assistance, resulting in an increase in cutting forces. On the other hand, rotary ultrasonic oscillation is along the z-axis, and its high-frequency oscillation can reduce the contact area in the cutting area. Simultaneously, it creates a vacuum region between the cutting tool and the workpiece material, facilitating air to enter the cutting area. This contributes to chip evacuation, reduced cutting forces, and lower cutting temperatures. Therefore, cutting forces with rotary ultrasonic assistance are the lowest among all the assistance methods. Compared to no assistance, rotary ultrasonic assistance can reduce cutting forces by approximately 16%.



**Figure 13.** Cutting force comparison among both different ultrasonic-assisted methods and without assistance for two sets of process parameters planned in the 1st phase of the experiment.

In this section, the laser locally preheating temperature is approximately 620 °C, which elevates the localized temperature of SKD11 to achieve material softening, resulting in mechanical properties that are distinct from those at room temperature, consequently reducing cutting forces. As shown in Figure 14, with the assistance of laser preheating, the hybrid assistance of laser, combined with rotary ultrasonic assistance, exhibits lower overall cutting forces compared to rotary ultrasonic assistance alone. In comparison to rotary ultrasonic assistance, the hybrid assistance of laser, combined with rotary ultrasonic assistance, can reduce cutting forces by up to 16%. Specifically, hybrid assistance demonstrates lower cutting forces at a spindle speed of 10,000 rpm, a radial depth of cut of 0.1 mm, and a feed rate of 1000 mm/min. Under fixed feed-rate conditions, cutting forces increase with the radial depth of cut. The trend of decreasing cutting forces is less apparent at a feed rate of 2000 mm/min, suggesting that an excessively rapid cutting feed rate may result in inadequate laser preheating due to the fixed laser irradiation point on the front edge of the cutting-tool and its movement with the worktable, causing insufficient preheating time and a less-noticeable reduction in cutting forces. Under fixed radial depth of cut conditions, cutting forces increase with the feed rate. It is inferred that a deeper radial depth of cut may lead to insufficient effective preheating depth by the laser, and the feed rate also affects the laser preheating temperature, resulting in inadequate preheating effects and, therefore, ineffective reduction in cutting forces.



**Figure 14.** Cutting force comparison between hybrid assistance and rotary assistance for process parameter combinations in an L9 orthogonal array.

#### 4.3. Machined Surface Morphology

After completing the milling experiments, the test samples were adequately cleaned and placed on a tool microscope with a 20× objective lens to observe the upper edge of the machined surface morphology. This section focuses on comparing the surface morphology under different process parameters along with rotary ultrasonic-assisted and hybrid-assisted methods in the second-phase of the experiment. Figure 15 shows the machined surface morphology comparisons for some specific combinations of process parameters and assisted milling methods. It can be observed that the machined surface morphology of the hybrid-assisted method performs better than the rotary ultrasonic-assisted method alone under the same process parameters. The rotary ultrasonic assistance method can reduce the contact area in the cutting zone and create a vacuum region between the cutting tool and the workpiece material, aiding chip evacuation and reducing cutting forces and temperature. This is beneficial because the high hardness and strength of SKD11 may lead to surface edge fracture or damage, especially at high feed rates. It can be observed that under high feed rates and large radial depths of cut, defects in the surface morphology are more pronounced. Under the same cutting process parameters, hybrid-assisted milling has a better surface morphology. This assistance combines the advantages of rotary ultrasonic assistance with the local softening of SKD11 by the laser

spot, providing better machinability. The maximum locally measured laser preheating temperature in this experiment is approximately 620 °C. According to reference [30], maintaining surface temperatures between 600 °C and 750 °C on SKD11 workpieces results in better machinability. Therefore, compared to rotary ultrasonic assistance alone, it can reduce the occurrence of surface edge defects. At a feed rate of 2000 mm/min, the surface edge of rotary ultrasonic assistance shows significant fracture and damage. In addition, with an increase in radial depth of cut, the defects in the surface morphology become more pronounced. At a feed rate of 1500 mm/min, a similar trend is observed. When the feed rate is reduced to 1000 mm/min, defects in the surface morphology become more apparent, with an increase in radial depth of cut. However, compared to feed rates of 2000 mm/min and 1500 mm/min, the defects are significantly reduced, and the integrity of the surface morphology is better. Increasing the feed rate leads to an increase in the number of cutting-tool edges engagement in the workpiece material per minute, enhancing cutting forces accordingly. Excessive cutting forces may cause vibration, resulting in more severe defects in the surface morphology. From Figure 15, it is evident that hybrid-assisted milling provides significantly better surface morphology integrity than rotary ultrasonic assistance alone. Although high feed rates and deeper radial depths of cut may affect the laser irradiation preheating time and preheating depth on SKD11, the hybrid assistance method achieves localized preheating and softening, resulting in a more complete surface morphology as compared to rotary ultrasonic assistance.

#### 4.4. Cutting-Tool Wear

After completing the milling experiments, the cutting tools were removed from the spindle system and cleaned, and they were placed on a tool microscope with a 10× objective lens to observe cutting-tool flank wear. The photographs of cutting-tool flank wear shown in Figure 16 for each experiment are all captured at the end of milling state, i.e., 70 mm milling distance. The comparison involved 18 milling cutters used in the Taguchi experiments, with two assisted methods. Different factors affecting cutting-tool wear were also investigated. From Figure 16, it can be observed that under rotary ultrasonic assistance, cutting-tool wear is more severe, with instances of broken and chipped cutting-tool edges. As the feed rate and depth of cut increase, rotary ultrasonic assistance shows larger areas of wear and breakage, following a similar trend to machined surface edge. At a feed rate of 2000 mm/min, the cutting tools under rotary ultrasonic assistance exhibit clear fracture and damage, and with an increase in radial depth of cut, the width of cutting-tool wear also significantly increases. At the radial depths of cut of 0.3 mm and 0.5 mm, severe fracture and chipping occur. At a radial depth of cut of 0.1 mm, the wear width and cutting-tool edge damage are reduced. At a feed rate of 1500 mm/min, an increase in radial depth of cut leads to a corresponding increase in cutting-tool wear width. However, as compared to a feed rate of 2000 mm/min, cutting-tool edge chipping and fracture are significantly reduced. At a feed rate of 1000 mm/min, the improvement in wear width and cutting-tool edge defects is most apparent. Under the same process parameters, hybrid-assisted milling shows a significant reduction in cutting-tool wear width and edge fracture. This is attributed to the localized preheating on SKD11 by laser assistance, providing better machinability. Additionally, the rotary ultrasonic oscillation factor shortens the contact time between the cutting-tool edge and the workpiece, reducing the load on the cutting-tool edge and effectively ejecting chips, reducing the occurrence of cutting-tool edge fracture and significantly extending cutting-tool life. However, at a feed rate of 2000 mm/min and radial depths of cut of 0.3 mm and 0.5 mm, there are still instances of cutting-tool edge fracture. In situations with deeper radial depths of cut and faster feed rates, preheating locally with laser has a shorter preheating time on the machined surface. Despite the local softening of the material, the preheating time and depth are insufficient, and the material's high hardness, combined with the dynamic load, cutting-tool debris, and material chip effects, result in faster cutting-tool wear during machining.

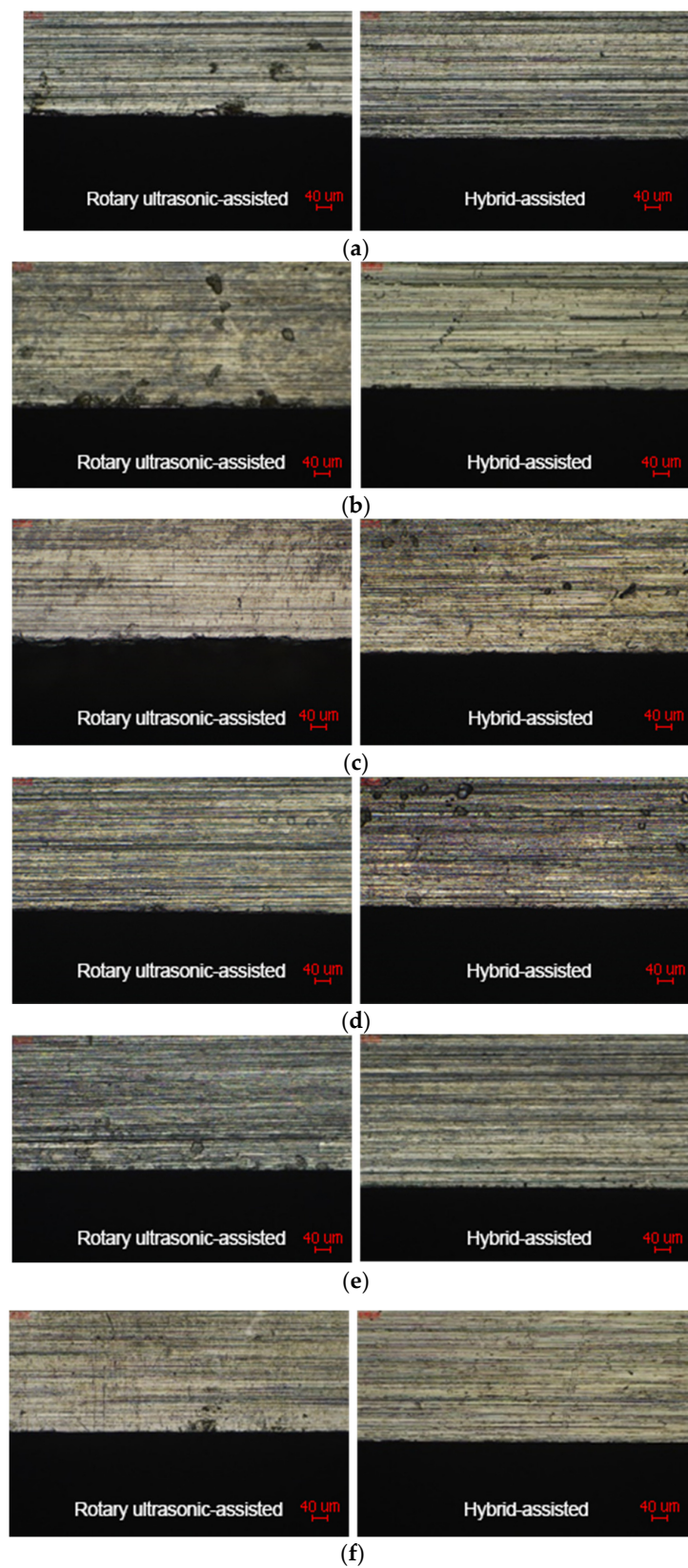


**Figure 15.** Machined surface morphology comparisons for some specific combinations of process parameter and assisted-milling methods: (a)  $n = 8000$ ,  $a_e = 0.5$  mm,  $F = 2000$  mm/min; (b)  $n = 10,000$ ,  $a_e = 0.5$  mm,  $F = 1500$  mm/min; (c)  $n = 9000$ ,  $a_e = 0.3$  mm,  $F = 2000$  mm/min; (d)  $n = 10,000$ ,  $a_e = 0.3$  mm,  $F = 1000$  mm/min; (e)  $n = 9000$ ,  $a_e = 0.1$  mm,  $F = 1500$  mm/min; (f)  $n = 8000$ ,  $a_e = 0.1$  mm,  $F = 1000$  mm/min.

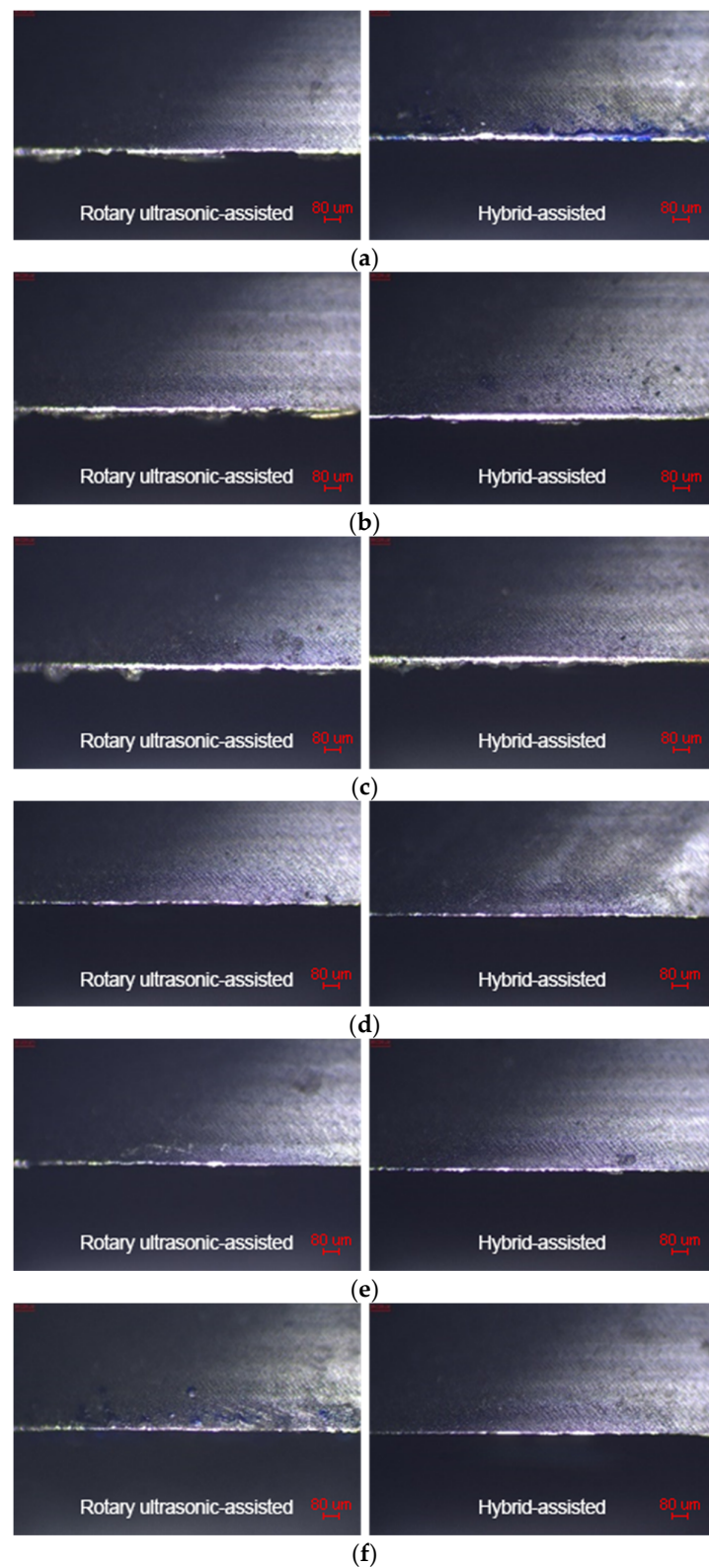


**Figure 16.** Cutting-tool wear comparisons for some specific combinations of process parameters and assisted milling methods: (a)  $n = 8000$ ,  $a_e = 0.5$  mm,  $F = 2000$  mm/min; (b)  $n = 10,000$ ,  $a_e = 0.5$  mm,  $F = 1500$  mm/min; (c)  $n = 9000$ ,  $a_e = 0.5$  mm,  $F = 1000$  mm/min; (d)  $n = 10,000$ ,  $a_e = 0.1$  mm,  $F = 2000$  mm/min; (e)  $n = 9000$ ,  $a_e = 0.1$  mm,  $F = 1500$  mm/min; (f)  $n = 8000$ ,  $a_e = 0.1$  mm,  $F = 1000$  mm/min.

#### 4.5. Machine Learning

The model training process involves hyperparameter tuning using the training dataset and evaluating the model through 5-fold cross-validation. The hyperparameter combination that performs the best is selected as the model's parameter configuration. Finally, the optimized base regression models, including decision tree (DT), random forest (RF), extra trees, XGBoost (XGB), LightGBM (LGBM), AdaBoost, stochastic gradient descent (SGD), support vector regressor (SVR), least squares support vector regressor (LSVR), and multi-layer perceptron (MLP), comprising ten models, are used to construct a voting regression model for predicting the test set. The predictive performance of different machine learning models is compared to assess whether there are differences in predictive performance between ensemble learning and individual machine learning models. The evaluation metrics used in this experiment include the coefficient of determination ( $R^2$ ), the root mean squared error (RMSE), the mean squared error (MSE), and the mean absolute error (MAE) to assess the model's performance.

The coefficient of determination (R-squared,  $R^2$ ) ranges between 0 and 1, with a value closer to 1 indicating that the model can fully explain all variations, while a value closer to 0 suggests that the model cannot explain any variations. A higher  $R^2$  implies a better predictive performance of the model. The relevant formula is given by Equation (2), where  $N$  represents the sample size,  $y_i$  represents the actual values,  $\hat{y}_i$  represents the predicted values, and  $\bar{y}$  denotes the mean of the actual values.

$$R^2 = 1 - \frac{\frac{1}{N} \sum_{i=1}^N (y_i - \hat{y}_i)^2}{\frac{1}{N} \sum_{i=1}^N (y_i - \bar{y})^2} \quad (2)$$

The mean squared error (MSE) is the average of the squared differences between actual values and predicted values. A smaller MSE indicates a better predictive performance of the model. The relevant formula is given by Equation (3), where  $N$  represents the sample size,  $y_i$  represents the actual values, and  $\hat{y}_i$  represents the predicted values.

$$\text{MSE} = \frac{1}{N} \sum_{i=1}^N (y_i - \hat{y}_i)^2 \quad (3)$$

The root mean square error (RMSE) is a commonly used evaluation metric in regression tasks. It is the square root of the average of the squared differences between actual values and predicted values. A smaller RMSE indicates a better predictive performance of the model. The relevant formula is given by Equation (4), where  $N$  represents the sample size,  $y_i$  represents the actual values, and  $\hat{y}_i$  represents the predicted values.

$$\text{RMSE} = \sqrt{\frac{1}{N} \sum_{i=1}^N (y_i - \hat{y}_i)^2} \quad (4)$$

The mean absolute error (MAE) is a commonly used evaluation metric in regression tasks. It is the average of the absolute differences between actual values and predicted values. A smaller MAE indicates a better predictive performance of the model. The relevant formula is given by Equation (5), where  $N$  represents the sample size,  $y_i$  represents the actual values, and  $\hat{y}_i$  represents the predicted values.

$$\text{MAE} = \frac{1}{N} \sum_{i=1}^N |y_i - \hat{y}_i| \quad (5)$$

##### 4.5.1. Machine Learning Results

In this section, machine learning metric scores are based on the results from the test dataset. Each model has different metric scores, as shown in Table 7 and Figure 17. The

decision tree (DT) model performs the worst among all models, with an  $R^2$  of 0.69132, RMSE of 0.58086, MSE of 0.3374, and MAE of 0.43112. This is speculated to be because the model is too simple to capture the complex relationships in the data. The extra trees model performs the best on all metrics, with an  $R^2$  of 0.91737, RMSE of 0.30053, MSE of 0.09032, and MAE of 0.21134. This is likely due to the introduction of more randomness and the fact that the model's generalization capability could be enhanced. Different models exhibit different performances, indicating that various machine learning models have distinct performance advantages. This can also be observed in Figure 18, which shows scatter plots for each regression model. It is evident that extra trees, AdaBoost, RF, and XGB have better predictive results, while DT and SVR perform poorly, with higher errors compared to other models. The figure also illustrates that each model has a different trend in predicting results.

**Table 7.** Performance comparisons among different machine learning models.

Models	Indicators	$R^2$	RMSE	MSE	MAE
DT		0.69132	0.58086	0.3374	0.43112
RF		0.90902	0.31534	0.09944	0.22303
Extra Trees		0.91737	0.30053	0.09032	0.21134
XGB		0.90144	0.32822	0.10773	0.22051
LGBM		0.78587	0.48379	0.23405	0.32589
AdaBoost		0.91051	0.31276	0.09782	0.23232
SGD		0.85313	0.40066	0.16053	0.2977
SVR		0.70355	0.56924	0.32403	0.36844
LSVR		0.81672	0.44758	0.20033	0.27107
MLP		0.88668	0.35195	0.12387	0.28653

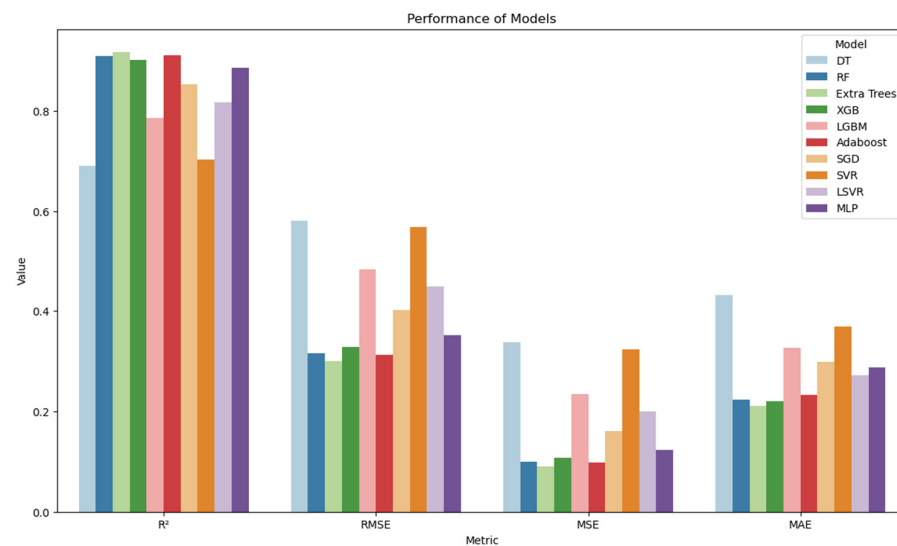


**Figure 17.** Performance comparisons among different machine learning models.

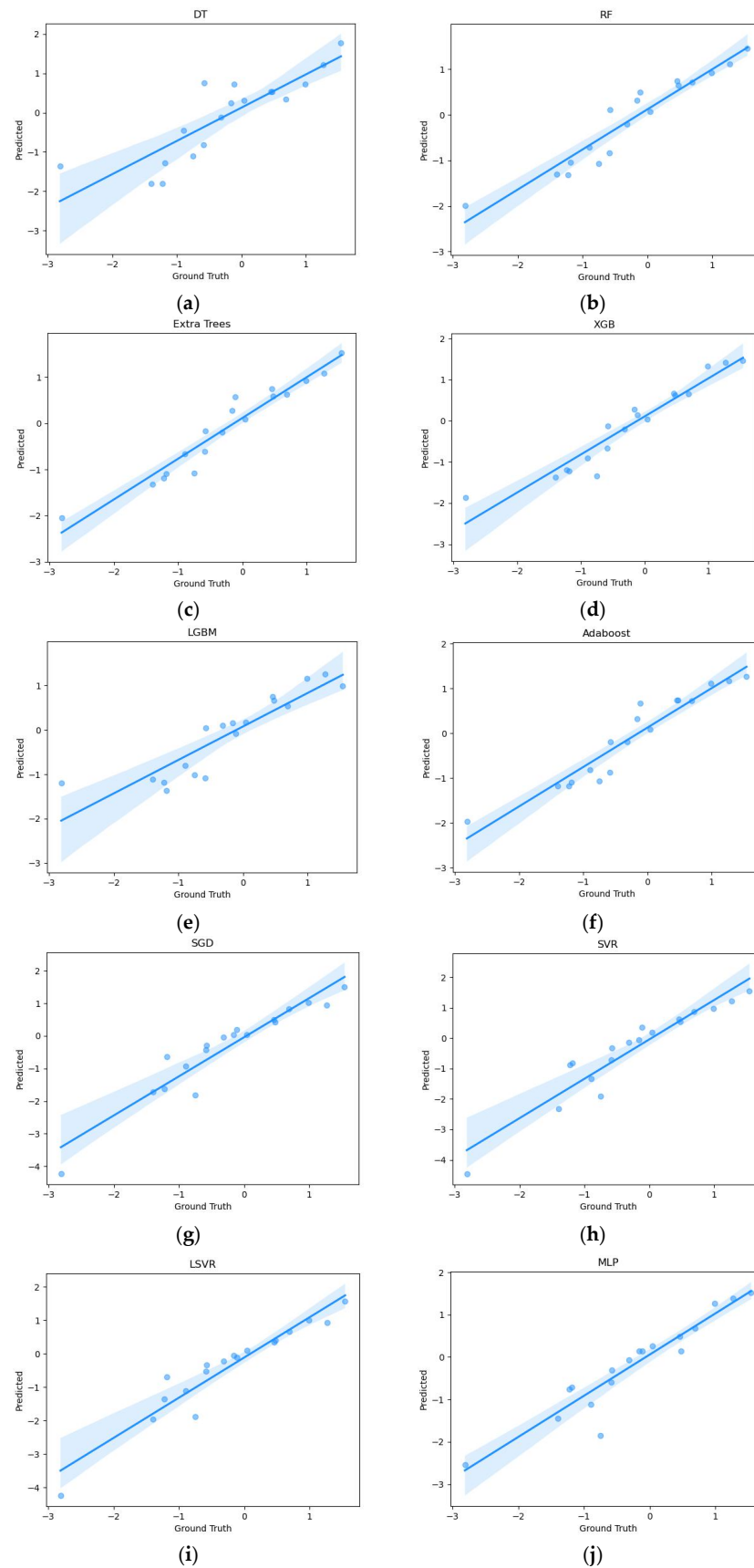


**Figure 18.** Scatter plots showing the relationship between predicted values and ground truth across different machine learning models: (a) DT, (b) RF, (c) extra trees, (d) XGB, (e) LGBM, (f) AdaBoost, (g) SGD, (h) SVR, (i) LSVR, (j) MLP.

#### 4.5.2. Machine Learning and Ensemble Learning Results

Similarly, the machine learning metric scores are based on the results from the test dataset in this section. The ensemble voting regression model, composed of the basic regression models, including DT, RF, extra trees, XGB, LGBM, AdaBoost, SGD, SVR, LSVR, and MLP, is constructed to predict the test dataset. It is compared with the best-performing model in all metrics from the machine learning models in Section 4.5.1, which is the extra trees model. As shown in Figure 19 and Table 8, the performance of the voting regression model surpasses that of the extra trees model. The extra trees model is the best-performing model among the ten basic regression models, indicating that the voting regressor outperforms other machine learning models. The metric scores for this model are an  $R^2$  of 0.94576, RMSE of 0.24348, MSE of 0.05928, and MAE of 0.18182. The residual plots in Figure 20 demonstrate that different models have distinct interpretations and levels of significance for the data. By combining multiple models, a better prediction of data characteristics can be achieved. Using multiple models allows for balance, even if one model’s predictive performance is poor; the results from the other models can help compensate, providing a more stable prediction. As shown in Figure 21, the residual values of the voting regression model are closer to the central 0 line on the horizontal axis compared to other models, indicating a more centered distribution.

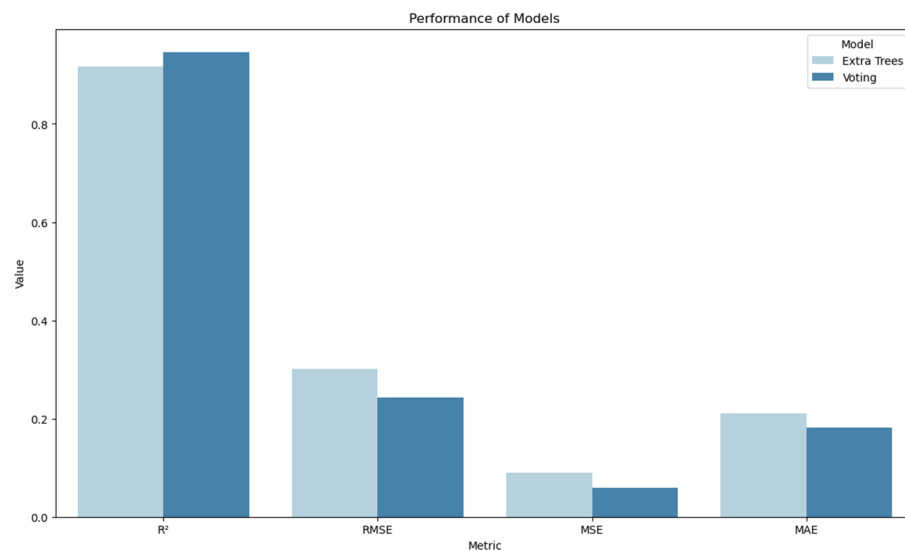


**Figure 19.** Performance comparisons between extra trees machine learning and ensemble learning models.

**Table 8.** Performance comparisons between extra trees machine learning and ensemble learning models.

Models	Support	$R^2$	RMSE	MSE	MAE
Extra Trees		0.91737	0.30053	0.09032	0.21134
Voting		0.94576	0.24348	0.05928	0.18182

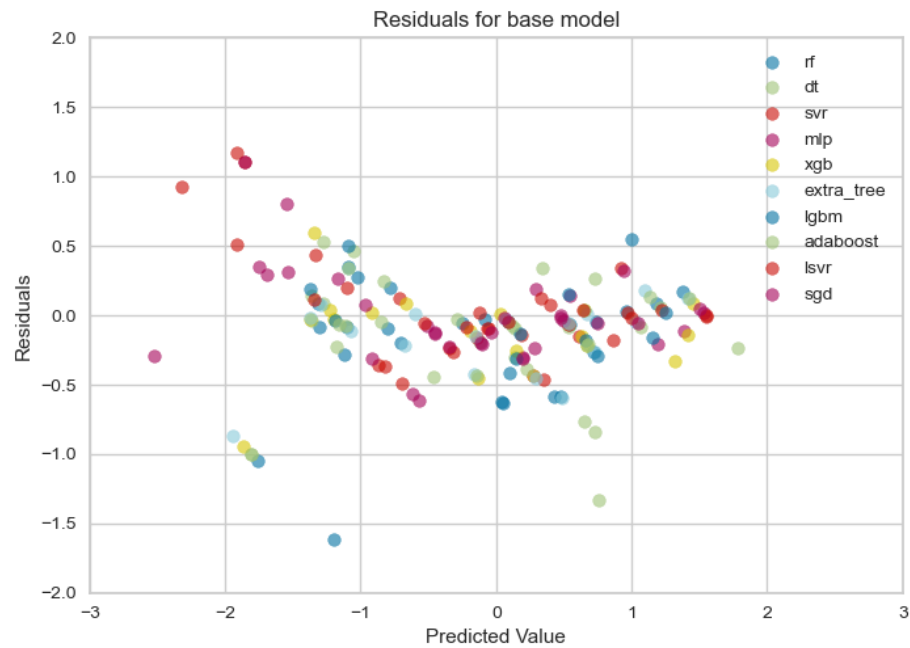


Figure 20. Relationship between residuals and predicted values for various machine learning models.

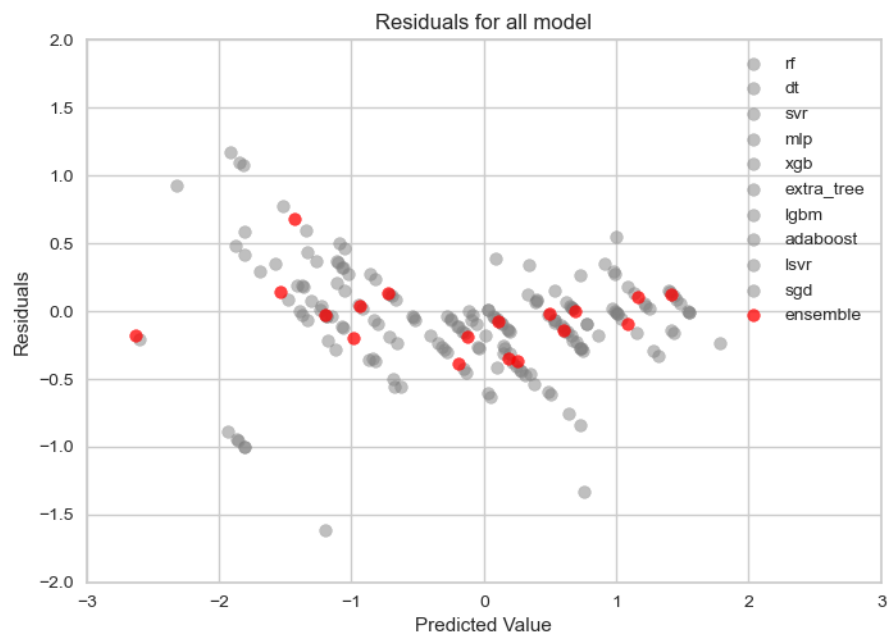


Figure 21. Relationship between residuals and predicted value for various machine learning models and ensemble learning model.

### 5. Conclusions

This study conducted side-milling experiments on SKD11 in two phases. The first phase aimed to explore the effects of different ultrasonic-assisted methods, including rotary, dual-axis and triple-axis, on milling performance. The better ultrasonic-assisted method obtained from the first phase was then adopted in the second phase both in conjunction with and without assistance from locally preheating with a laser, in which the Taguchi orthogonal array was applied for milling process parameter planning. The surface roughness and cutting-tool life served as the objective function and constraint, respectively, and the optimal combination of process parameters was thus determined by the characteristics of the smaller-the-better in the Taguchi method. Based on the optimal milling process parameters obtained and the superior hybrid-assisted method adopted, milling experiments

were repeatedly performed to collect the data of cutting force and cutting-tool wear. An ensemble learning method was applied to construct a cutting-tool wear prediction model after the data underwent the processes of cleaning, feature extraction, data standardization, and feature selection. From the above analyses, the following conclusions can thus be drawn:

1. As various ultrasonic-assisted methods compared with no assisted milling in the first phase experiments, it was found that ultrasonic-assisted machining could improve machining quality, reduce cutting force, and enhance surface roughness. Among them, rotary ultrasonic-assisted showed the best cutting performance.
2. As compared to the method without assisted milling, the rotary-assisted ultrasonic method could reduce surface roughness by approximately 5% and cutting force by 16%. When compared to rotary ultrasonic assistance, hybrid-assisted milling could reduce surface roughness by 30% and cutting force by 16%.
3. Among the multiple machine learning models in this study, extra trees exhibited the best performance, with an  $R^2$  of 0.91737, RMSE of 0.30053, MSE of 0.09032, and MAE of 0.21134.
4. The ensemble voting regression model for cutting-tool wear prediction on the test dataset, can achieve an  $R^2$  of 0.94576, RMSE of 0.24348, MSE of 0.05928, and MAE of 0.18182.
5. As compared to all the individual regression models in this study, the ensemble voting regression model exhibited the best generalization capabilities. This method can integrate the complementary predictive capabilities among different individual models and its generalization capabilities can be enhanced by combining the strengths of the multiple models. Therefore, ensemble machine learning is a feasible and effective method for monitoring cutting-tool wear.

**Author Contributions:** Conceptualization, supervision, writing, S.-Y.L.; methodology, analysis, C.-J.H. All authors have read and agreed to the published version of the manuscript.

**Funding:** This research received no external funding.

**Institutional Review Board Statement:** Ethical review and approval were waived for this study since it did not involve research with living organisms.

**Informed Consent Statement:** Not applicable.

**Data Availability Statement:** Correspondence and requests for materials should be addressed to Shen-Yung Lin. The data are not publicly available due to patent in review.

**Acknowledgments:** The authors acknowledge the National Formosa University for their support in this research.

**Conflicts of Interest:** The authors declare no conflicts of interest.

## References

1. Abellan-Nebot, J.V.; Subirón, F.R. A review of machining monitoring systems based on artificial intelligence process models. *Int. J. Adv. Manuf. Technol.* **2010**, *47*, 237–257. [\[CrossRef\]](#)
2. Liang, S.Y.; Hecker, R.L.; Landers, R.G. Machining process monitoring and control: The state-of-the-art. *J. Manuf. Sci. Eng.* **2004**, *126*, 297–310. [\[CrossRef\]](#)
3. Anderson, M.; Patwa, R.; Shin, Y.C. Laser-assisted machining of Inconel 718 with an economic analysis. *Int. J. Mach. Tools Manuf.* **2006**, *46*, 1879–1891. [\[CrossRef\]](#)
4. Mejbil, M.K.; Khalaf, M.M.; Kwad, A.M. Improving the machined surface of AISI H11 tool steel in milling process. *J. Mech. Eng. Res. Dev.* **2021**, *44*, 58–68.
5. Tsai, M.Y.; Chang, C.T.; Ho, J.K. The machining of hard mold steel by ultrasonic assisted end milling. *Appl. Sci.* **2016**, *6*, 373. [\[CrossRef\]](#)
6. Ding, H.; Ibrahim, R.; Cheng, K.; Chen, S.-J. Experimental study on machinability improvement of hardened tool steel using two dimensional vibration-assisted micro-end-milling. *Int. J. Mach. Tools Manuf.* **2010**, *50*, 1115–1118. [\[CrossRef\]](#)
7. Gao, H.; Ma, B.; Zhu, Y.; Yang, H. Enhancement of machinability and surface quality of Ti-6Al-4V by longitudinal ultrasonic vibration-assisted milling under dry conditions. *Measurement* **2022**, *187*, 110324. [\[CrossRef\]](#)

8. Kumar, M.; Melkote, S.N. Process capability study of laser assisted micro milling of a hard-to-machine material. *J. Manuf. Process.* **2012**, *14*, 41–51. [[CrossRef](#)]
9. Brecher, C.; Emonts, M.; Rosen, C.-J.; Hermani, J.-P. Laser-assisted milling of advanced materials. *Phys. Procedia* **2011**, *12*, 599–606. [[CrossRef](#)]
10. Woo, W.-S.; Lee, C.-M. A study of the machining characteristics of AISI 1045 steel and Inconel 718 with a cylindrical shape in laser-assisted milling. *Appl. Therm. Eng.* **2015**, *91*, 33–42. [[CrossRef](#)]
11. Wang, C.; Ding, F.; Tang, D.; Zheng, L.; Li, S.; Xie, Y. Modeling and simulation of the high-speed milling of hardened steel SKD11 (62 HRC) based on SHPB technology. *Int. J. Mach. Tools Manuf.* **2016**, *108*, 13–26. [[CrossRef](#)]
12. Wang, C.Y.; Xie, Y.X.; Qin, Z.; Lin, H.S.; Yuan, Y.H.; Wang, Q.M. Wear and breakage of TiAlN-and TiSiN-coated carbide tools during high-speed milling of hardened steel. *Wear* **2015**, *336–337*, 29–42. [[CrossRef](#)]
13. Gong, F.; Zhao, J.; Ni, X.; Liu, C.; Sun, J.; Zhang, Q. Wear and breakage of coated carbide tool in milling of H13 steel and SKD11 hardened steel. *SN Appl. Sci.* **2019**, *1*, 1111. [[CrossRef](#)]
14. Pu, Z.; Singh, A. High speed ball nose end milling of hardened AISI A2 tool steel with PCBN and coated carbide tools. *J. Manuf. Process.* **2013**, *15*, 467–473. [[CrossRef](#)]
15. Gong, F.; Zhao, J.; Jiang, Y.; Tao, H.; Li, Z.; Zang, J. Fatigue failure of coated carbide tool and its influence on cutting performance in face milling SKD11 hardened steel. *Int. J. Refract. Met. Hard Mater.* **2017**, *64*, 27–34. [[CrossRef](#)]
16. Twardowski, P.; Czyżycki, J.; Felusiak-Czyryca, A.; Tabaszewski, M.; Wiciak-Pikuła, M. Monitoring and forecasting of tool wear based on measurements of vibration accelerations during cast iron milling. *J. Manuf. Process.* **2023**, *95*, 342–350. [[CrossRef](#)]
17. Niu, B.; Sun, J.; Yang, B. Multisensory based tool wear monitoring for practical applications in milling of titanium alloy. *Mater. Today Proc.* **2020**, *22*, 1209–1217. [[CrossRef](#)]
18. Mahmood, J.; Mustafa, G.-E.; Ali, M. Accurate estimation of tool wear levels during milling, drilling and turning operations by designing novel hyperparameter tuned models based on LightGBM and stacking. *Measurement* **2022**, *190*, 110722. [[CrossRef](#)]
19. Zhou, H.; Gao, S.; Xie, Y.; Zhang, C.; Liu, J. Multi-condition wear prediction and assessment of milling cutters based on linear discriminant analysis and ensemble methods. *Measurement* **2023**, *216*, 112900. [[CrossRef](#)]
20. Kilundu, B.; Dehombreux, P.; Chimentin, X. Tool wear monitoring by machine learning techniques and singular spectrum analysis. *Mech. Syst. Signal Process.* **2011**, *25*, 400–415. [[CrossRef](#)]
21. Huang, Z.; Shao, J.; Guo, W.; Li, W.; Zhu, J.; Fang, D. Hybrid machine learning-enabled multi-information fusion for indirect measurement of tool flank wear in milling. *Measurement* **2023**, *206*, 112255. [[CrossRef](#)]
22. Çınar, Z.M.; Nuhu, A.A.; Zeeshan, Q.; Korhan, O.; Asmael, M.; Safaei, B. Machine learning in predictive maintenance towards sustainable smart manufacturing in industry 4.0. *Sustainability* **2020**, *12*, 8211. [[CrossRef](#)]
23. Sarker, I.H. Machine learning: Algorithms, real-world applications and research directions. *SN Comput. Sci.* **2021**, *2*, 160. [[CrossRef](#)] [[PubMed](#)]
24. Sagi, O.; Rokach, L. Ensemble learning: A survey. *Wiley Interdiscip. Rev. Data Min. Knowl. Discov.* **2018**, *8*, e1249. [[CrossRef](#)]
25. Elbestawi, M.; Papazafiriou, T.; Du, R. In-process monitoring of tool wear in milling using cutting force signature. *Int. J. Mach. Tools Manuf.* **1991**, *31*, 55–73. [[CrossRef](#)]
26. Kuljanic, E.; Sortino, M. TWEM, a method based on cutting forces—Monitoring tool wear in face milling. *Int. J. Mach. Tools Manuf.* **2005**, *45*, 29–34. [[CrossRef](#)]
27. Gierlak, P.; Burghardt, A.; Szybicki, D.; Szuster, M.; Muszyńska, M. On-line manipulator tool condition monitoring based on vibration analysis. *Mech. Syst. Signal Process.* **2017**, *89*, 14–26. [[CrossRef](#)]
28. Qin, Y.; Liu, X.; Yue, C.; Zhao, M.; Wei, X.; Wang, L. Tool wear identification and prediction method based on stack sparse self-coding network. *J. Manuf. Syst.* **2023**, *68*, 72–84. [[CrossRef](#)]
29. Mao, X.; Zhang, F.; Wang, G.; Chu, Y.; Yuan, K. Semi-random subspace with Bi-GRU: Fusing statistical and deep representation features for bearing fault diagnosis. *Measurement* **2021**, *173*, 108603. [[CrossRef](#)]
30. Xavierrockiaraj, S.; Kuppan, P. Investigation of cutting forces, surface roughness and tool wear during Laser assisted machining of SKD11Tool steel. *Procedia Eng.* **2014**, *97*, 1657–1666. [[CrossRef](#)]

**Disclaimer/Publisher’s Note:** The statements, opinions and data contained in all publications are solely those of the individual author(s) and contributor(s) and not of MDPI and/or the editor(s). MDPI and/or the editor(s) disclaim responsibility for any injury to people or property resulting from any ideas, methods, instructions or products referred to in the content.